

56 Copies

NATIONAL AERONAUTICS AND SPACE ADMINISTRATION

Technical Report 32-1284

Temperature Control of the Mariner Venus 67
Spacecraft

L. N. Dumas

GPO PRICE \$ _____

CSFTI PRICE(S) \$ _____

Hard copy (HC) _____

Microfiche (MF) _____

ff 653 July 65

FACILITY FORM 602

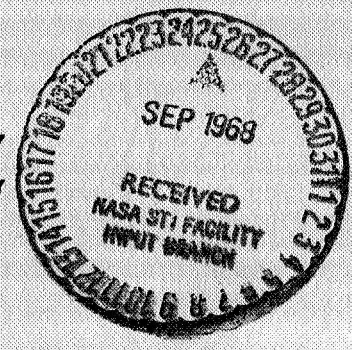
(ACCESSION NUMBER) NC 34070 (THRU) _____

56 (PAGES) _____ (CODE) _____

CR-96708 (NASA CR OR TMX OR AD NUMBER) _____ (CATEGORY) 31

JET PROPULSION LABORATORY
CALIFORNIA INSTITUTE OF TECHNOLOGY
PASADENA, CALIFORNIA

July 15, 1968



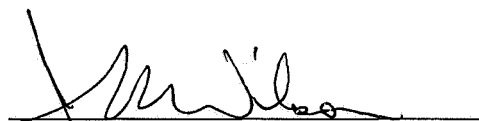
NATIONAL AERONAUTICS AND SPACE ADMINISTRATION

Technical Report 32-1284

*Temperature Control of the Mariner Venus 67
Spacecraft*

L. N. Dumas

Approved by:

A handwritten signature in black ink, appearing to read 'J. N. Wilson', is written over a horizontal line.

J. N. Wilson, Manager
Mariner Development Section

JET PROPULSION LABORATORY
CALIFORNIA INSTITUTE OF TECHNOLOGY
PASADENA, CALIFORNIA

July 15, 1968

JPL TECHNICAL REPORT 32-1284

Copyright © 1968

Jet Propulsion Laboratory
California Institute of Technology

Prepared Under Contract No. NAS 7-100
National Aeronautics & Space Administration

PRECEDING PAGE BLANK NOT FILMED.

Acknowledgment

The author is indebted to Mr. D. C. Miller and Mr. R. A. Becker, who contributed to the design and development of the temperature control subsystem, to Mr. H. D. von Delden, who designed the thermal shields and sun shade, and to Mr. W. F. Carroll, who provided materials support for temperature control hardware. These engineers, who deserve much of the credit for the success of the temperature control subsystem, offered valuable assistance in the preparation of this report. Mr. von Delden drafted the material from which the sections on subsystem hardware were taken. Mr. J. D. Schmuecker reviewed the manuscript and made suggestions leading to improvements in format and content. The author remains responsible for any errors.

Contents

I. Introduction	1
II. Design Approach	3
III. Design Requirements and Description	3
A. Solar Panel View Factor Reduction	4
B. Deployable Sun Shade	6
IV. Hardware Description	6
A. Louvers	6
B. Side Shields	8
C. Thermal Blankets	8
D. Deployable Sun Shade	11
E. Attitude Control Jet Shields	14
F. Trapped Radiation Detector Shield	14
G. Magnetometer Shield	14
H. Surface Coatings and Treatments	15
I. Temperature Control References	15
J. Thermal Shield Containers	15
V. Test Program	16
A. Temperature Control Model	16
B. Flight Spacecraft	18
1. The M67-1	18
2. The M67-2	19
VI. Analysis	19
VII. Flight Results	20
A. Launch	22
B. Midcourse Maneuver	22
C. Encounter	32
D. Cruise	32
VIII. Conclusions and Recommendations	34
Appendix A. Project Organization	36

Contents (contd)

Appendix B. Flight Transducer Locations	38
--	----

References	47
-----------------------------	----

Tables

1. Temperature limits	3
2. Temperature control surfaces	15
3. Summary of test data (°F) for M67-1	16
4. Summary of test data (°F) for M67-2	19
5. Telemetered flight temperatures (°F), predicted and actual	21

Figures

1. <i>Mariner Mars 1964</i> spacecraft	1
2. <i>Mariner Venus 67</i> spacecraft	2
3. Bay-face to solar-panel view factor	4
4. Sun shade coverage	5
5. <i>Mariner V</i> on Agena adapter	7
6. Arrangement of louvers, side shields, and exposed painted surfaces	9
7. Upper thermal shield	11
8. Lower thermal shield	12
9. Sun shade in stowed position	13
10. Sun shade in deployed position	13
11. Sun shade retainer	13
12. Sun shade release lanyard	14
13. TCM in JPL 10-ft space simulator	17
14. Analytical nodal network	20
15. Solar intensity at <i>Mariner V</i> spacecraft	22
16. Bay 1 flight temperature, channel 401	23
17. Bay 3 flight temperature, channel 402	23
18. Bay 2 flight temperature, channel 421	23
19. PIPS propellant tank flight temperature, channel 217	23
20. PIPS N ₂ tank flight temperature, channel 408	23

Contents (contd)

Figures (contd)

21. Bay 4 flight temperature, channel 423	23
22. Trapped radiation detector flight temperature, channel 438	24
23. Bay 5 flight temperature, channel 404	24
24. Voltage controlled oscillator flight temperature, channel 424	24
25. Tape recorder flight temperature, channel 436	24
26. Bay 6 flight temperature, channel 405	24
27. Auxiliary oscillator 1 flight temperature, channel 414	24
28. Auxiliary oscillator 2 flight temperature, channel 418	24
29. Bay 7 flight temperature, channel 426	25
30. +X/−Y attitude control N ₂ tank flight temperature, channel 218	25
31. −X/+Y attitude control N ₂ tank flight temperature, channel 219	25
32. Bay 8 flight temperature, channel 407	25
33. Canopus sensor flight temperature, channel 410	25
34. Battery flight temperature, channel 428	25
35. UV photometer flight temperature, channel 437	26
36. Upper thermal shield flight temperature, channel 434	26
37. High gain antenna flight temperature, channel 419	26
38. Low gain antenna mast flight temperature, channel 431	26
39. Magnetometer flight temperature, channel 439	26
40. Lower thermal shield flight temperature, channel 435	26
41. Lower thermal shield degradation	27
42. Plasma probe flight temperature, channel 422	27
43. Primary sun sensor flight temperature, channel 430	27
44. +X roll and yaw jet assembly flight temperature, channel 406	27
45. −Y pitch jet assembly flight temperature, channel 425	27
46. −X roll and yaw jet assembly flight temperature, channel 433	28
47. I _{sc} − V _{oc} solar cell flight temperature, channel 403	28
48. Solar panel spar flight temperature, channel 427	28
49. Solar panel flight temperatures, channels 409 and 429	28
50. Midcourse transient temperatures for antennas and magnetometer	29
51. Midcourse transient temperatures for propulsion subsystem	30
52. Midcourse transient temperatures for bays 1 and 3	30

Contents (contd)

Figures (contd)

53. Midcourse transient temperatures for primary sun sensor	31
54. Midcourse transient temperatures for UV photometer	31
A-1. Project organization	37
B-1. Temperature transducer	38
B-2. Typical electronics assembly installation	39
B-3. Bay 2 shear plate	39
B-4. Propellant tank	40
B-5. Propulsion nitrogen tank	40
B-6. Trapped radiation detector	41
B-7. Electronics assembly V	41
B-8. Electronics assembly VI	41
B-9. Attitude control nitrogen tanks	41
B-10. Electronics assembly VIII	41
B-11. Canopus sensor	42
B-12. Battery	42
B-13. UV photometer	42
B-14. Upper thermal shield	42
B-15. High gain antenna	43
B-16. Omni mast	44
B-17. Magnetometer	44
B-18. Lower thermal shield	44
B-19. Plasma probe	44
B-20. Primary sun sensor	45
B-21. Temperature control references	45
B-22. Solar panel	46

Abstract

On October 19, 1967, the *Mariner V* spacecraft successfully encountered Venus and obtained scientific information about the planet. The variation in solar intensity during the mission made effective solar isolation a requirement for spacecraft survival. The temperature control design is presented, with emphasis on the design features which provided this isolation. The results of thermal testing and flight temperature data are summarized and discussed.

Temperature Control of the Mariner Venus 67 Spacecraft

I. Introduction

The *Mariner Venus 67* Project was initiated in December 1965 with the intent of conducting a flyby mission to Venus in 1967 to obtain scientific information about the planet. Also obtained were engineering experience in converting and operating a spacecraft designed for flight to Mars into one for flight to Venus, and information on the interplanetary environment during a period of increasing solar activity. Accordingly, spacecraft survival through encounter plus ten ($E + 10$) days was mandatory, and survival through perihelion was desirable. The greatest possible use was made of residual *Mariner Mars 1964* equipment and testing techniques. The spacecraft was fully automatic and attitude-stabilized, using the sun and the star Canopus as attitude references. The scientific equipment payload included a trapped radiation detector, plasma probe, magnetometer, ultraviolet photometer, and a dual-frequency receiver. The spacecraft weight at launch was 540 pounds; the height was 113 in., the *wingspan* was 219 in., and the primary spacecraft structure (octagonal bus) was 51 in. across flats and 18 in. high. Virtually all spacecraft electronics were housed within the bus. Outside this main compartment were appended solar panels, scientific sensors, attitude control devices, and antennas. Figure 1 shows the general configuration of *Mariner Mars 1964*; Fig. 2 shows *Mariner Venus 67*.

Before launch, the flight spacecraft *Mariner V* was designated M67-2. It was the reworked flight spare from

the *Mariner Mars 1964* program, when it was known as MC-4. Other residual 1964 hardware was assembled into still another spacecraft which served as a prototype and flight spare for the 1967 mission. This spacecraft, the first of those assembled and tested, was designated M67-1. Unlike preceding *Mariner* missions, which provided for the launching of two identical spacecraft within a few days of each other, the 1967 Venus mission called for a single launching.

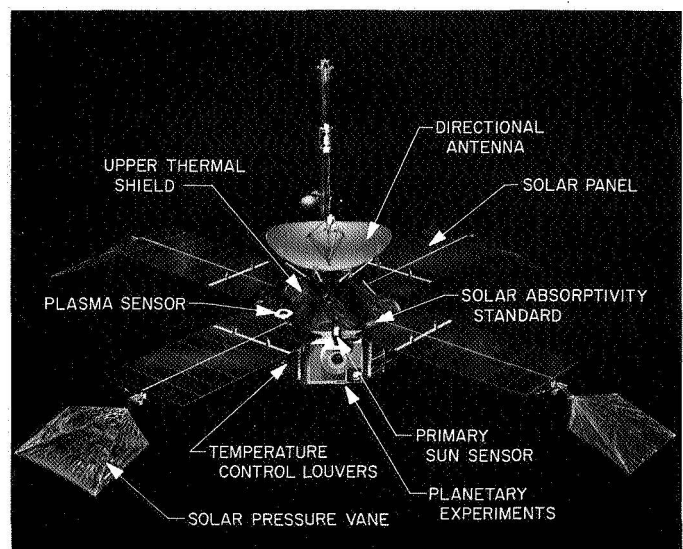


Fig. 1. *Mariner Mars 1964* spacecraft

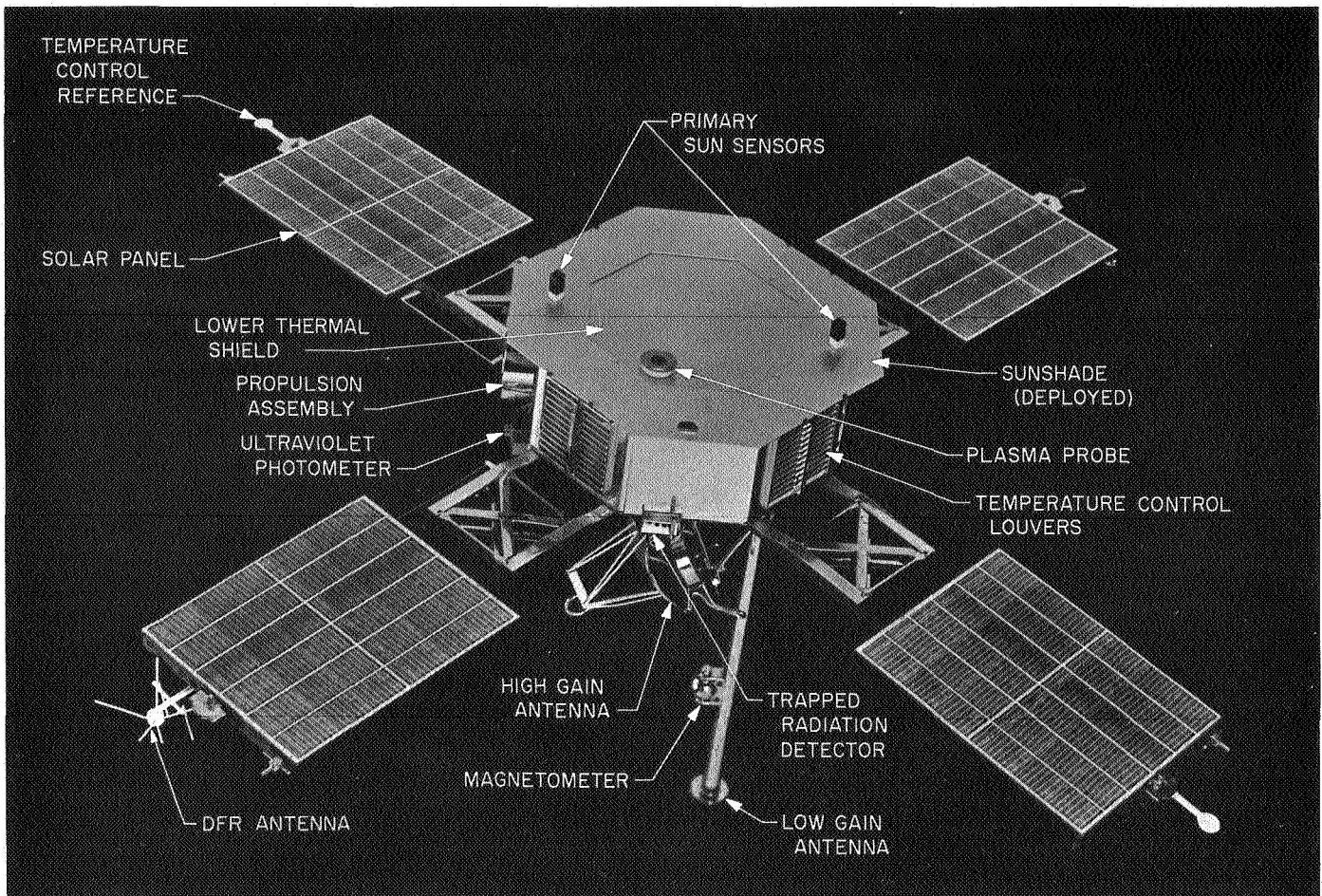


Fig. 2. Mariner Venus 67 spacecraft

The *Mariner V* spacecraft was launched into heliocentric orbit on June 14, 1967. Planetary encounter occurred on October 19, where gravitational influence of Venus deflected the trajectory of the craft toward the sun. The spacecraft transmitter was switched from high to low gain antenna on November 21, 1967, and the last telemetry was obtained at that time. Perihelion, at 0.58 AU solar distance, occurred on January 4, 1968 (Refs. 1, 2).

The thermal design of the *Mariner Venus 67* spacecraft was similar in concept to that of preceding *Mariner* missions (Refs. 3, 4, 5), which included *Mariner II* (Venus 1962) and *Mariner IV* (Mars 1964). The *Mariner II* design was marginal: for most electronics at Venus encounter the temperature ranged from 120° to 150°F. The spacecraft failure three weeks after encounter was due at least in part to overheating. The *Mariner IV* design was considerably more successful (Ref. 6). Spacecraft temperatures remained within tolerance for more than

three years in space (Ref. 7). Significant changes to this design were required to successfully complete a Venus mission, however.

The flight spacecraft for the 1967 Venus mission was to be the reworked flight spare from the *Mariner Mars* 1964 program. Changes within the bus were relatively minor, so little modification of the internal thermal design was required. The important thermal differences between the 1964 and 1967 missions were boundary condition changes. Because of antenna pointing requirements, *Mariner V* was flown *upside down* relative to the sun as compared with *Mariner IV*. The second significant boundary condition change was the greatly increased solar intensity at the *Mariner V* spacecraft, which was 126 W/ft² at launch, 248 W/ft² at encounter, and 386 W/ft² at perihelion. The critical thermal problems of the *Mariner Venus 67* spacecraft concerned the control of the external heat balance in such a way that acceptably cool spacecraft temperatures would result.

II. Design Approach

The design approach for the temperature control subsystem was that of both test and analysis, with perhaps more emphasis on space simulator tests and less emphasis on analysis than is usual. Early in the program a simplified thermal analysis computer model was generated. From this model and *Mariner* Mars 1964 experience, a preliminary design was then derived. The design was verified — and modified as necessary — during space simulator testing of a full scale temperature control model. Spacecraft temperature response to various input parameters was also empirically obtained during these tests. From these results, the computer model was revised for use in the prediction of flight temperatures in situations that could not be simulated (i.e., launch, midcourse, and encounter transients). Space simulator testing of the flight spacecraft provided additional cruise temperature data, which (after correction for known test errors) formed the basis for flight predictions. Minor modifications to the thermal design were made during these tests to provide final adjustments in temperature.

Thus the *Mariner* Venus 67 philosophy was to use test data whenever possible for both design purposes and flight predictions. This philosophy stems from the nature of the *Mariner* flyby missions. Because of scientific and

long-range communications requirements, these spacecraft are three-axis stabilized so that the orientation to the sun is unchanging. The interplanetary trajectories traveled take the spacecraft beyond the thermal influence of the earth about an hour after launch, and encounter geometries are such that the spacecraft temperatures are only mildly affected by the planetary encounter. Hence the greater part of the spacecraft flight is spent in a quasi-equilibrium condition with solar heating the only significant external heat input. Furthermore, for the *Mariner* Venus 67 design every effort was made to minimize the influence of solar heating on most of the spacecraft. Thus the spacecraft had relatively simple boundary conditions and was insensitive to solar spectrum and intensity. These factors combined to make the *Mariner* space simulator tests both straightforward and generally accurate. The single-launch nature of the 1967 mission demanded the utmost in reliability, and the design approach taken was considered the most conservative method available.

III. Design Requirements and Description

Table 1 lists allowable temperature ranges for the spacecraft. *Operating* and *nonoperating* limits were design goals; *flight acceptance* (FA) and *type approval*

Table 1. Temperature limits

Assembly	Operating limit, °F		Nonoperating limit, °F		Flight acceptance, °F		Type approval, °F	
	Min	Max	Min	Max	Min	Max	Min	Max
Bay 1 (power)	14	167	14	167	32	131	14	167
Bay 2 (propulsion)	35	125	35	125	32	131	14	167
Bay 3 (science)	14	122	-20	122	32	131	14	167
Bay 4 (data encoder)	14	167	14	167	32	131	14	167
Bay 5 (receiver and tape)	14	149	14	167	32	131	14	167
Bay 6 (transmitter)	14	167	0	167	32	131	14	167
Bay 7 (attitude control)	30	131	14	167	32	131	14	167
Bay 8 (power)	14	167	14	167	32	131	14	167
Battery	40	140	14	140	32	131	14	167
Solar panels	-175	175	-175	200	75	240	40	284
Sun sensors	30	130	-20	160	32	131	14	167
Canopus sensor	0	100	-30	128	0	100	14	167
Magnetometer	-40	131	-40	149	-40	122	-50	167
Trapped radiation detector	-4	122	-22	100	-4	122	14	122
UV photometer	32	149	0	167	32	131	14	167
Plasma probe	-58	302	-58	302	32	239	14	275

(TA) limits were prescribed test values. Temperature control standards were normally based on design limits. Limits are shown at the assembly or structural level. Individual components may exceed these limits because of internal power dissipation and resulting temperature gradients. Temperature control, as a discipline, concerned the maintenance of acceptable spacecraft temperatures down to the subassembly (module) level. Except in special cases, component temperature control was accomplished as part of the packaging design. When unusual design problems were encountered, as in the case of the radio traveling wave tube and solar panel zener diodes, analytical and test support was provided.

Temperature limits for structure and independently mounted components outside the bus were generally broad enough to permit the application of passive temperature control techniques. Optical property control, local shades, and emittance shields were used in conventional fashion. Wherever possible, temperature-sensitive components were conductively coupled with the bus to maintain an acceptable temperature range (e.g., attitude control sensors). Fixed shades were used over the trapped radiation detector and the attitude control jet assemblies to reduce direct solar heating. An open-loop, 3-W heater was used to warm the magnetometer.

In the bus, the lower temperature limits were dictated by the midcourse motor propellant freezing point of 34°F and by the degradation of the battery performance below 40°F. Materials deterioration under long term storage at elevated temperatures in the tape recorder and propulsion subsystems defined the maximum allowable bus temperature. A design goal of 40° to 80°F within the bus was established for cruise during the primary mission (from launch to Venus encounter plus ten ($E + 10$) days. To stay within this temperature range, the bus had to be shielded as much as possible from solar heating. The fixed solar attitude of the spacecraft permitted the use of a multilayered thermal shield on the sunlit side of the bus to provide most of the necessary protection. A similar thermal shield on the opposite (shaded) side of the bus minimized uncontrolled heat losses and internal temperature gradients. The internal heat dissipation of 140 to 250 W, and unavoidable solar inputs, were rejected mainly through variable emittance louvers located on six of the eight bay faces. Temperature differences between bays were reduced by providing good internal radiation and conduction heat paths.

Two significant departures from the *Mariner Mars 1964* design to further reduce solar heating of the bus are discussed below.

A. Solar Panel View Factor Reduction

The radiant flux falling on a bay face from the corresponding panel is directly proportional to the bay-face-to-panel view factor and to the solar intensity. Since the solar intensity at encounter for the *Mariner Venus 67* spacecraft was about twice the maximum *Mariner Mars 1964* level, the irradiation of the bay face would have scaled up proportionately had the panel design of *Mariner Mars 1964* been retained. The removal of side shielding to cool the bay would have aggravated the problem by exposing more area to the variable radiation from the panels. To reduce the bay-face-to-panel view factor, the celled area of the solar panel was moved away from the bus. The resultant effect of increasing the clearance is shown in Fig. 3. With the configuration as flown, the irradiation of the near bay from each solar panel was only about 4 W/ft² at encounter.

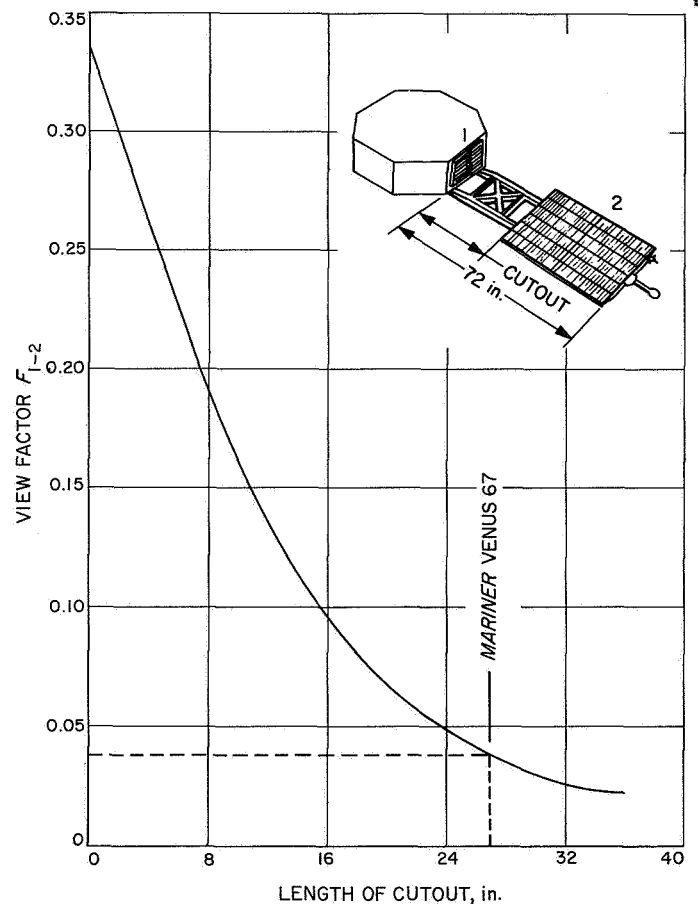


Fig. 3. Bay-face to solar-panel view factor

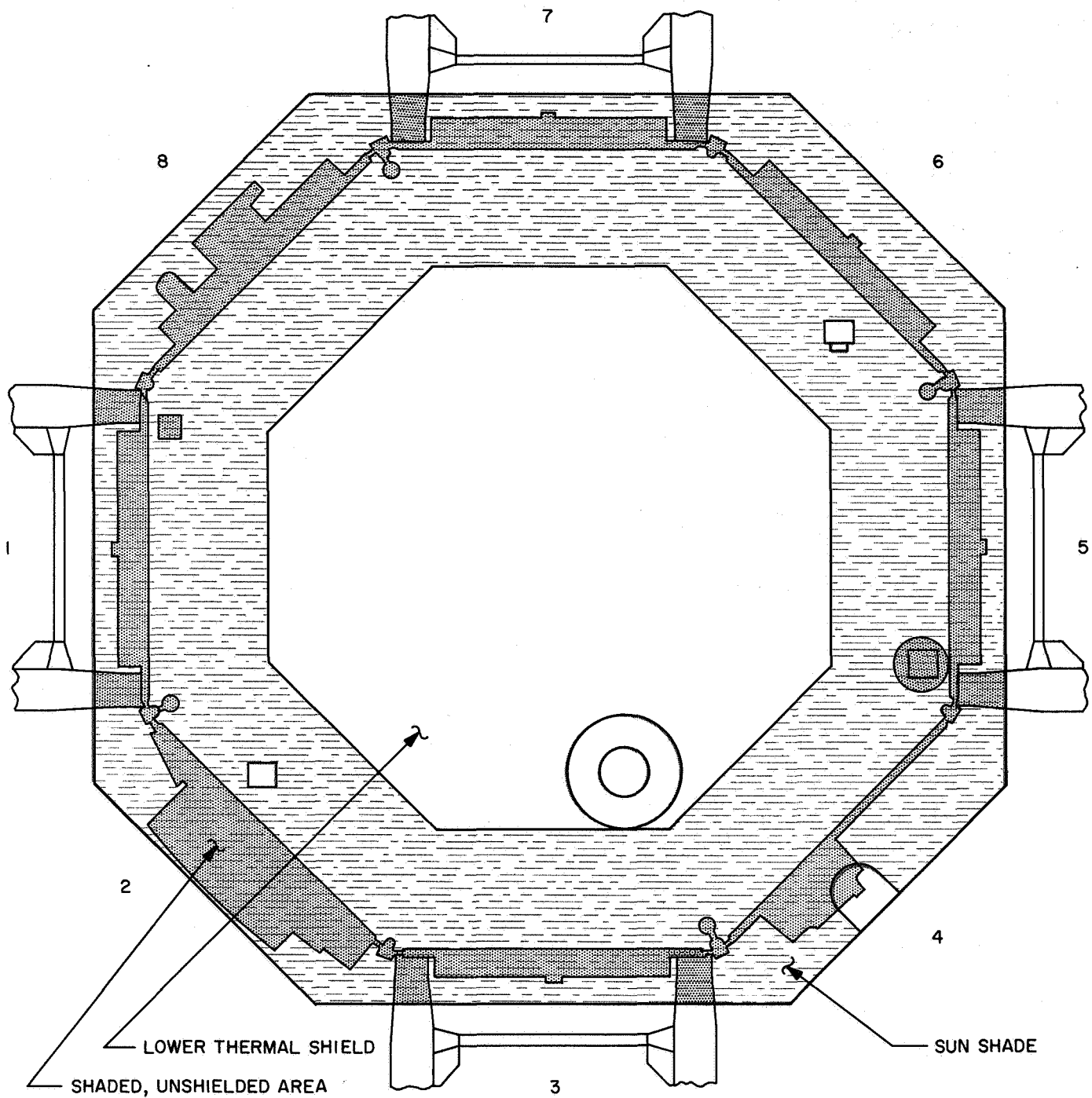


Fig. 4. Sun shade coverage

B. Deployable Sun Shade

The most significant single change from the *Mariner* Mars 1964 thermal design was the addition of a deployable sun shade. This shade protected the bus from sun heat inputs by shading three areas of potential solar heating:

- (1) Components mounted on the lower ring, which were functionally required to penetrate the lower (sunlit) shield, including electrical and mechanical interfaces with the launch vehicle adapter.
- (2) Structures which extended outboard of the bay faces, including the midcourse motor cover, Canopus sensor baffle box, trapped radiation detector, louver assemblies, and the umbilical connector.
- (3) Thermal shorts in the lower thermal shield caused by seams, edge attachments, support structure pressure, and other compromises necessary for fabrication.

The protected areas are illustrated in Fig. 4. Analyses of space simulator test data revealed that absorption by the bus of an incremental 150 W at Venus solar intensity with the shade stowed raised the average bus temperature by 33°F.

Estimated heat inputs to the bus are tabulated for earth and Venus cruise modes.

Source	Earth input, W	Venus input, W
Internal power dissipation	160	160
Conduction from plasma probe	1.5	2.5
Solar input to sun sensors	9	21
Conduction from solar panels	-8	-5
Radiation from solar panels	7	18
Input through sun shade and lower thermal shield	18.5	36
Net input to bus	188	232.5

IV. Hardware Description

The temperature control subsystem for the *Mariner* Venus 67 spacecraft comprised the thermal control hardware that was not an integral part of other subsystems. This classification included thermal shields, louver assemblies, temperature control references, and the sun shade; but excluded paints, conversion coatings, temperature transducers, and extra thickness built into hardware to increase conduction. By this admittedly arbitrary definition, the total subsystem weight was 17.0 lb, or 3.15% of the total spacecraft weight, and was broken down as follows:

Louver assemblies	8.1 lb
Fixed shields	3.7
Upper shield	2.0
Lower shield	1.8
Sun shade	1.1
Temperature control reference	0.3
Total subsystem	17.0 lb

A. Louvers

The *Mariner* Venus 67 variable emittance louvers were mounted on six of the seven electronic bays. Figure 5 shows typical louver installations on the flight spacecraft. Each louver assembly weighed 1.35 lb and covered an area of 1.62 sq ft. The effective emittance varied from 0.15 to 0.7 over a 30°F actuation range. Incipient opening was 55°F on bays 7 and 8, 60°F elsewhere. Eleven pairs of louver blades on each assembly were individually controlled by means of a spiral, bi-metallic element.

The louvers that remained from the *Mariner* Mars 1964 program were used for *Mariner* Venus 67. The only change to the louvers was the inclusion of sun shade lanyard guides that were bonded to the upper and lower corners of the actuator housing cover to prevent the lanyards from becoming entangled in the louvers. The louver design of the *Mariner* Mars 1964 is discussed in Ref. 8. The louvers were disassembled, cleaned, inspected, and subjected to the thermal portion of the flight acceptance test before redelivery to the Spacecraft Assembly Facility (SAF). Because of the questionable nature of the louver position indicator performance of the *Mariner IV*, these measurements were omitted in *Mariner V*.



Fig. 5. Mariner V on Agena adapter

B. Side Shields

Polished aluminum side shields were used on electronic bays to control the effective emitting area. These shields were fabricated from 12-mil sheeting. No attempt was made to thermally decouple the shield and bay face. The low emittance area provided by the aluminum was used to adjust the *set point* temperature for the bus. Figure 6 shows the arrangement of shielding used. No new hardware was required because sufficient residual side shields were available from *Mariner* Mars 1964.

C. Thermal Blankets

The upper and lower thermal shields were constructed of multiple layers of ½-mil Mylar aluminized on both sides. Alternate sheets of the same material were spacers that had been corrugated by the Dimplar process. These flexible blankets, about ½-in. thick, were faced with 1-mil aluminized Teflon with the Teflon side out. The lower (sunlit) blanket had a total of 19 layers; the upper (shaded) blanket had 13 layers. The lower shield was attached to the spacecraft with bolt-on angle brackets sewn to the shield. The upper shield was attached with Nylon hook-and-pile strips (Velcro) for ease in installing and removing. The corresponding *Mariner* Mars 1964 shield used metal brackets sewed to the blanket. The *Mariner* Venus 67 attachment method reduced the installation time and minimized the danger of damage that might occur during installation after final systems test and solar panel installation. The upper shield is shown in Fig. 7, the lower shield is shown in Fig. 8.

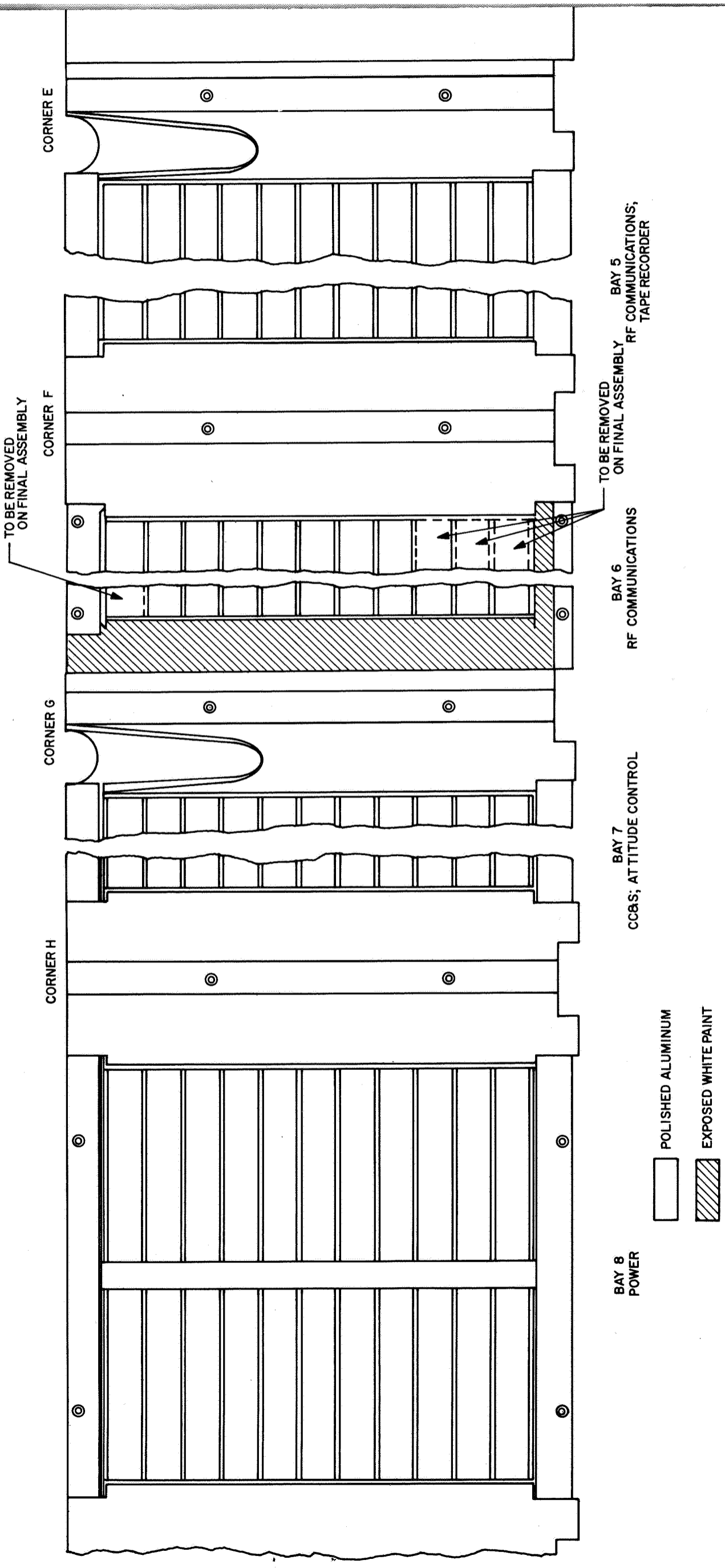
The gross difference in thermal environment of a mission to Venus from that of a mission to Mars dictated a change of material in the sunlit outer layer of the lower thermal shield. An α/ϵ ratio significantly lower than the black fabric used on *Mariner* Mars 1964 was required to avoid exceeding the upper temperature limit (300°F) of the Mylar in the shield. Of the films available, Mylar and Tedlar were known to darken under solar ultraviolet irradiation while Kapton and FEP Teflon appeared to be acceptably stable. Kapton had a higher initial solar absorptance, its availability in requisite widths was uncertain, and metallizing techniques were unproved at the time. Aluminized FEP Teflon, type A, had been extensively tested and had been successfully used on *Mariner II*, *Ranger*, *Surveyor*, and *Mariner IV*. This film can be aluminized, although adhesion is not high, and it is available in standard thicknesses from ½ to 20 mil. When aluminized, the film acts as a second surface mir-

ror yielding emittance values between 0.5 and 0.8 (increasing with thickness) and corresponding values of solar absorptance from 0.12 to 0.20. Minimum temperatures and minimum degradation would be expected for the thicker film. However, since spacecraft temperatures were insensitive to outer layer temperature, the 1-mil film was selected for the blanket and sun shade for facilitating deployment and handling.

Pre-dimpled Mylar (Dimplar) was selected for the thermal shields because of its light weight and crush resistance. The hand-crikkled Mylar used for *Mariner* Mars 1964 shields was known to be pressure-sensitive, so that thermal *shorts* existed at blanket supports and at other unavoidable points of bearing stress. It was desirable for the sake of shield efficiency and consistency of performance that such effects be minimized. The effective conductance for an uncompromised Dimplar shield is fairly high compared with some available multilayered systems, but this property is not important for *Mariner*-type shields whose overall properties are controlled by the effect of seams, penetrations, and edge attachments. A prototype lower shield was constructed to demonstrate feasibility of fabrication, and the decision to fly Dimplar was made without recourse to comparative thermal tests. This calculated risk was necessitated by limited time, manpower, and money. Tests of the temperature control model later confirmed the adequacy of the Dimplar shields.

The pre-dimpled Mylar was ½ mil thick and was processed with heat to form a permanent dimple or corrugation in the material. Several depths of deformation were investigated. Material with 3-6% *take up* was found to have the best mechanical properties. The 5-6% material had the best unit loading capability while the 3-4% material retained its configuration best. A shield fabricated with nine layers (alternately dimpled and flat) of material was 0.62-0.75 in. thick, while a thirty-layer shield of hand-wrinkled ¼-mil mylar was approximately 0.35 in. thick. In one test, after the two samples were compressed to approximately 0.062-in. thickness, the pre-dimpled material returned to 100% of its original height while the hand-wrinkled material returned to only 50%. The unit loading required to compress the samples was approximately ten times more for pre-dimpled samples than for the hand-wrinkled.

The pre-dimpled and the flat ½-mil Mylar were aluminized on both sides. This eliminated any requirement for inspection during fabrication to identify the aluminized side. The ½-mil material was much easier to



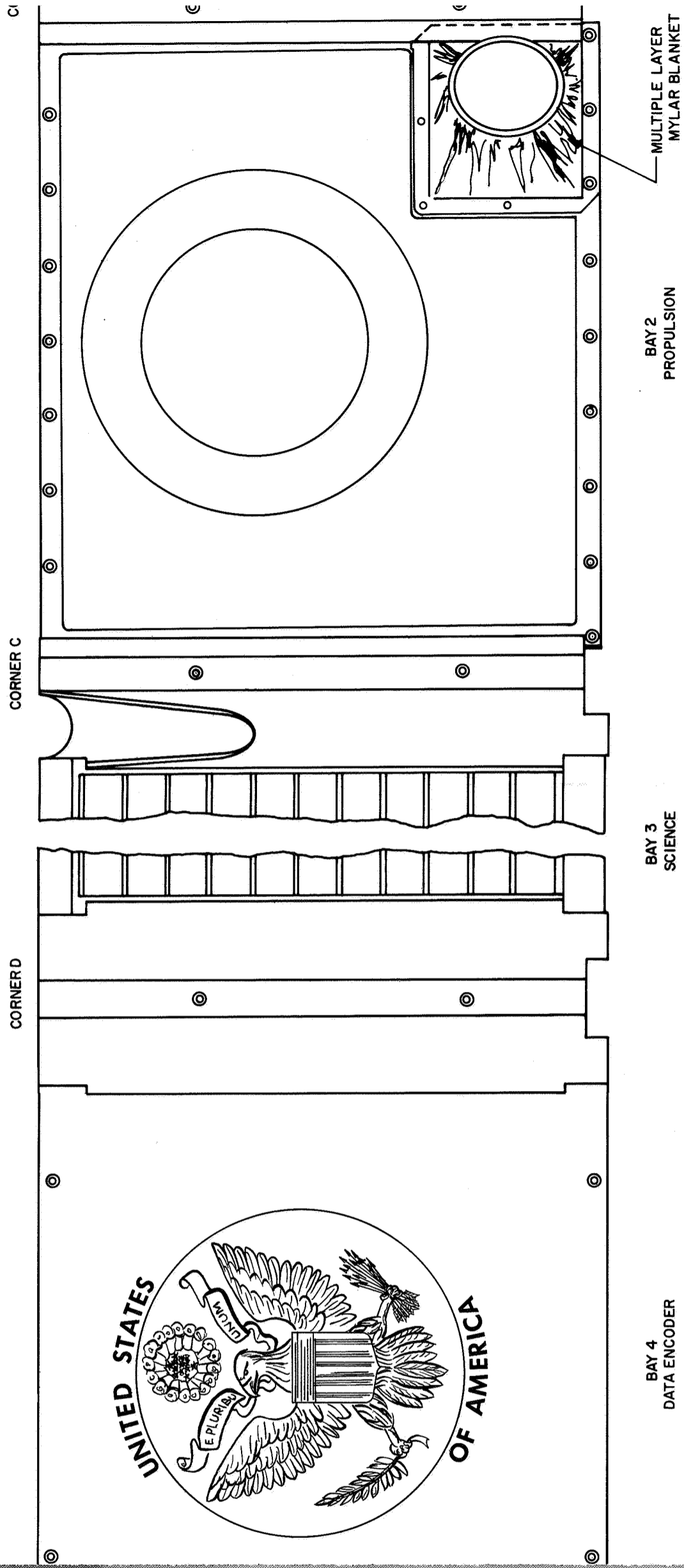
Fold-out #1

Fig. 6-17

P-9-A

Fig. B
P-9-B

PART A



FOLD-OUT #2

Fig. C
P-9-B

Fig. 6-D

PART B

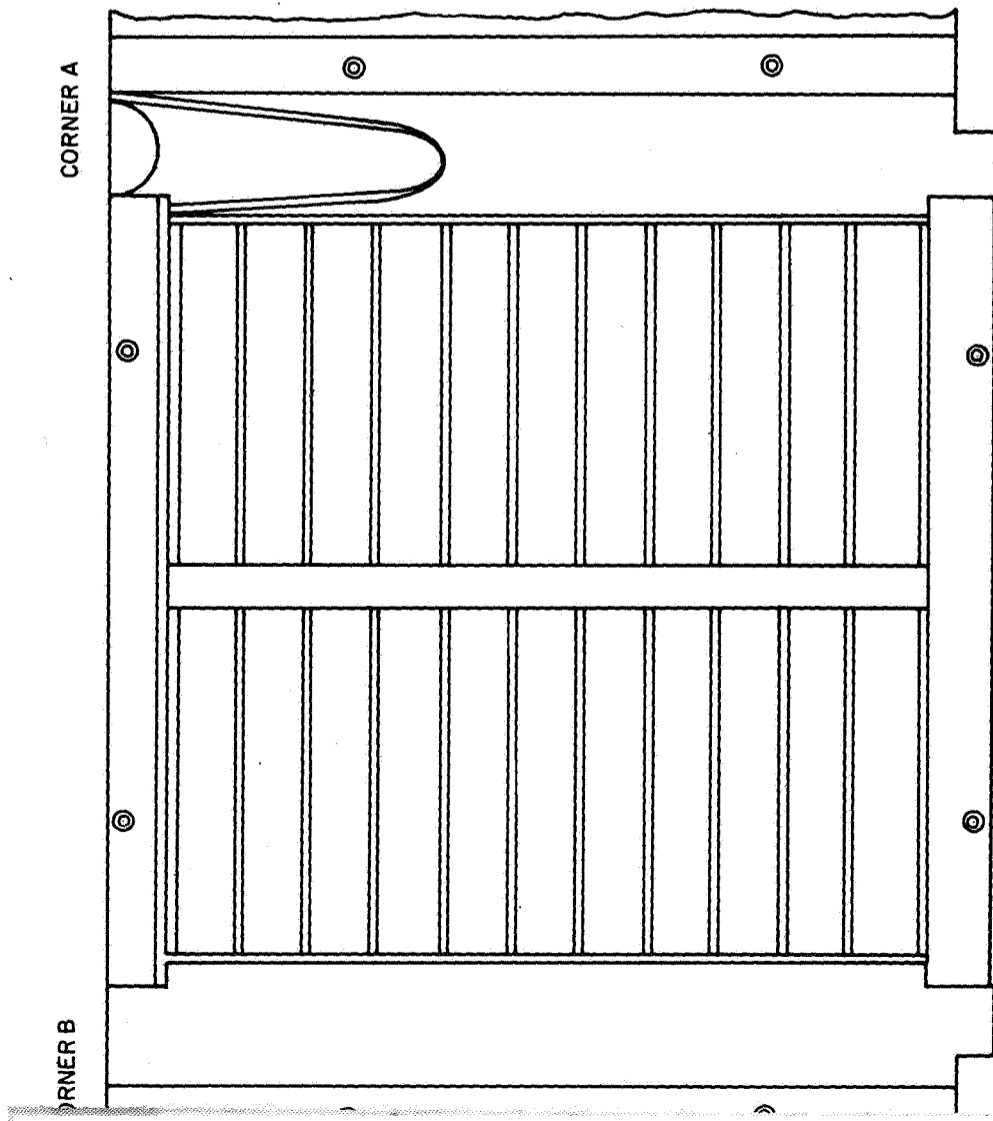


Fig. 6. Arrangement of louvers, side shields, and exposed painted surfaces

Fig. 6.E 9
P. 9-E



Fig. 7. Upper thermal shield

handle during the blanket fabrication although added difficulties arose in finishing because of the thickness. The pattern and detail fabrication techniques developed for the *Mariner* Mars 1964 program (Ref. 1) were used for the *Mariner* Venus 67 shield construction. One area requiring close attention was the limited capability of the paper pattern to contour as the thicker and more flexible finished thermal shield would. In many cases a small sample of the actual blanket material was used to arrive at the proper flat pattern necessary for fabrication.

D. Deployable Sun Shade

The deployable sun shade was fabricated from a single sheet of 1-mil Teflon aluminized on the side away from the sun. During launch, the shade was retracted to clear the *Agona* adapter and spacecraft interface hardware (Fig. 9). When deployed, the shade formed an octagonal awning approximately 10 in. wide around the periphery of the spacecraft, with a total area of about 1900 in². The deployment and support of the shade was performed by eight spiral-wound spring assemblies located on the four solar panel bays. A lanyard was

attached to a support rod between the pairs of springs in each of these bays and in turn through a series of eyelets to the corresponding solar panel. Each of these four sections of the shade was thereby deployed independently by the solar panel deployment in that bay. A 4-in.-diam clearance hole was provided at bay 4 so that the x-ray tube of the trapped radiation detector could have an unobstructed view of the sun. In the deployed position (Fig. 10), the shade extended beyond the edge of the bus approximately three inches in bays 1, 3, 5 and 7 and five inches in bays 2, 4, 6 and 8. The shade was symmetrical to balance solar pressure and simplify construction. The sun shade assembly contained 123 parts, including fasteners.

- (1) *Construction and assembly details.* An octagonal tubular support ring was sewn to the shade at the inner perimeter. The outside edge of the shade was hemmed to contain the four support tubes and a circumferential dacron cord. All of the shade edges were reinforced with a glass-backed aluminum tape to prevent tearing. Eight pieces of nylon hook (0.625 by 1 in.) were sewn to the

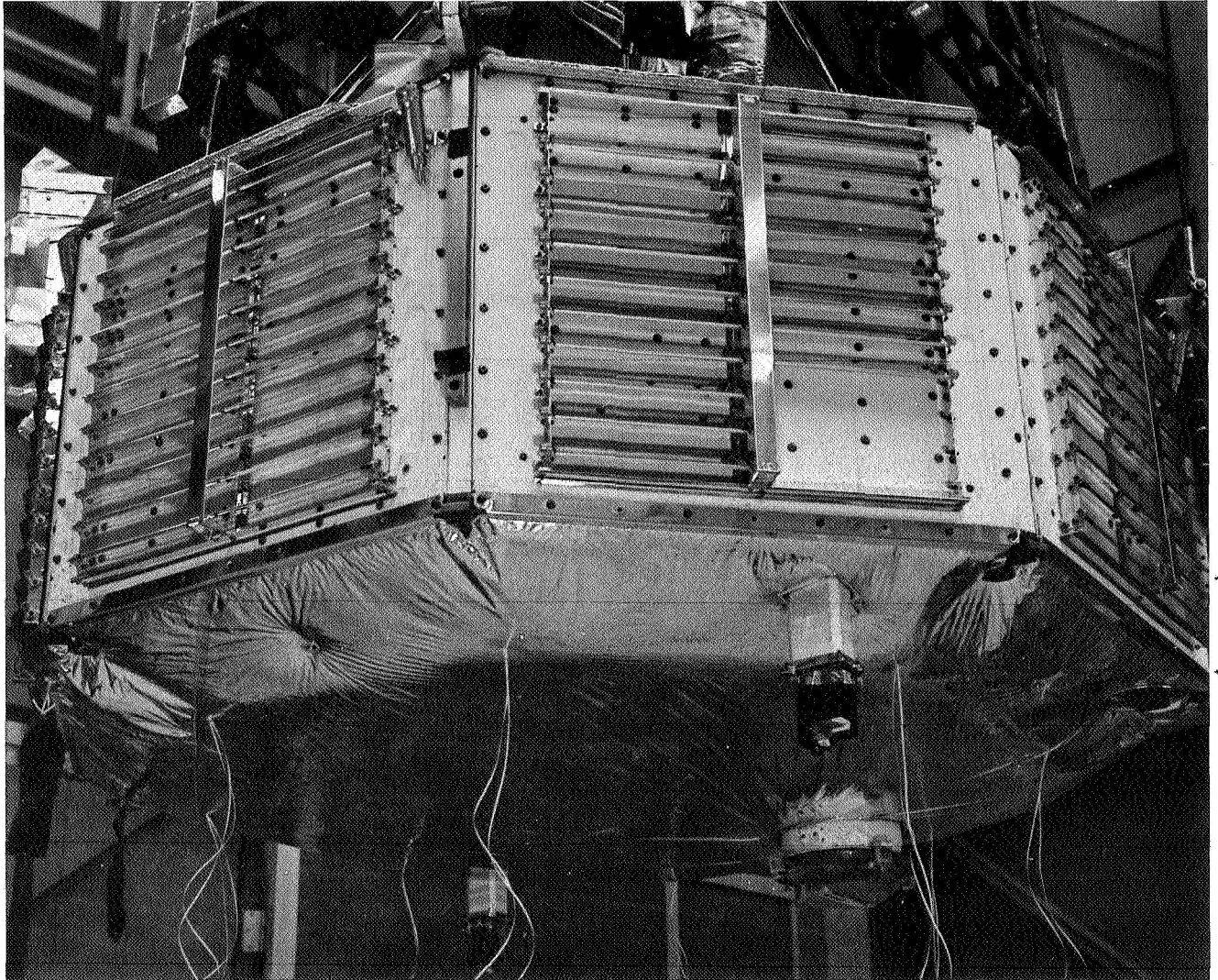


Fig. 8. Lower thermal shield

Teflon. When the shade was stowed, these mated with nylon hook retainers which extended from the deployment spring assemblies, thus preventing the shade from slipping from its stowed position.

The shade octagonal support ring was attached to the spacecraft by eight dacron ties that secured it through the lower thermal shield to the lower shield support ring. The four support tubes were attached to deployment spring assemblies that were in turn attached to the lower chassis screws in bays 1, 3, 5, and 7. When stowed, the loose shade material was folded and retained by mating nylon hook pads in bays 1, 3, 5, and 7. In bays 2, 4, 6, and 8 the excess material (*shirt tail*) was folded and retained by a $\frac{1}{4}$ -in.-diam Teflon ball

and clip. The Teflon ball was tied to a 2-in. dacron cord on the shade; the ball retainer clip was attached to the center lower chassis screw in each even numbered bay. The retainer clip was calibrated at installation to release the ball when a tension of 140 ± 10 grams was applied (see Fig. 11).

- (2) *Deployment.* The deployment and support of the shade was performed by eight spiral-wound spring assemblies located in pairs that attached to shade support tubes in bays 1, 3, 5, and 7. Each spring assembly contained a nonmagnetic, high strength Elgiloy steel spring mounted on an adjustable center arbor. Before their installation on the spacecraft, the spring assemblies in free position were pre-set to a torque of $1 \text{ in.-lb} \pm 2 \text{ in.-oz}$. The

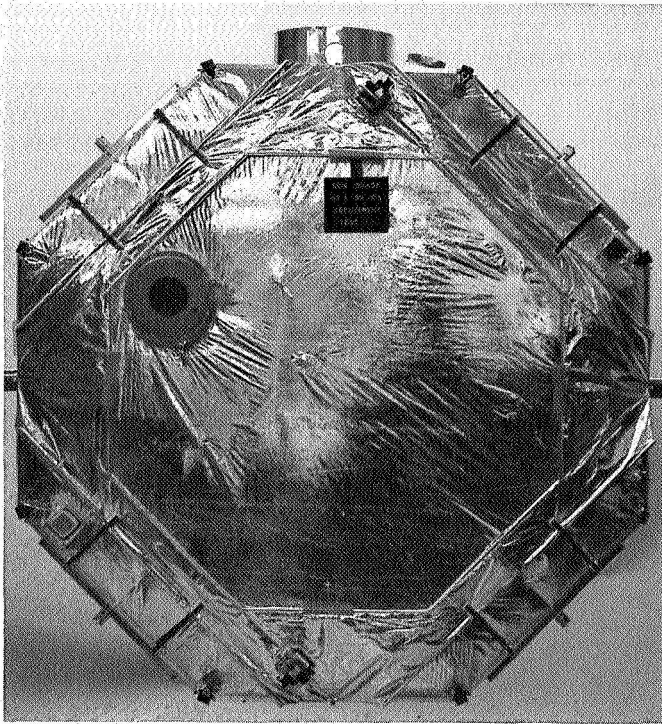


Fig. 9. Sun shade in stowed position

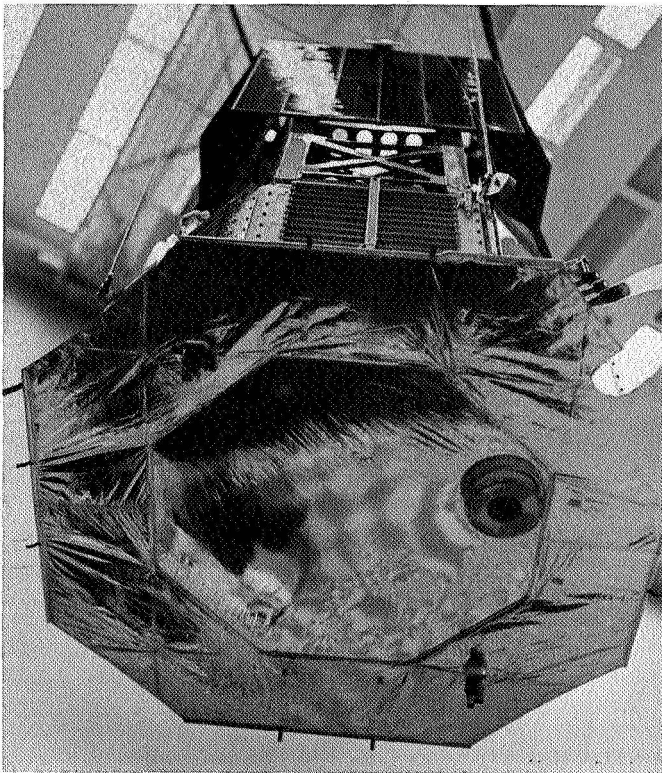


Fig. 10. Sun shade in deployed position

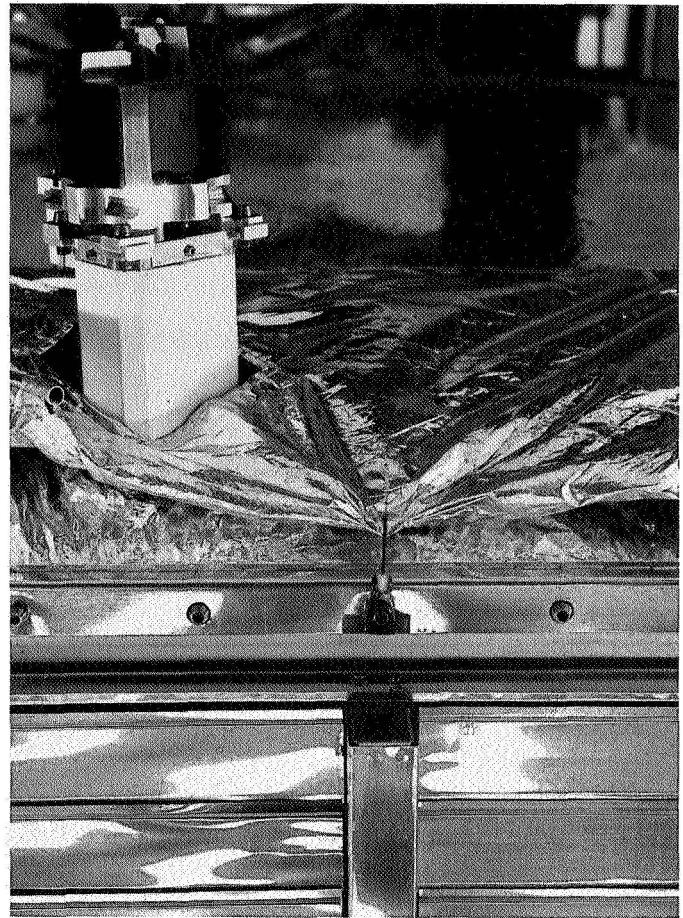


Fig. 11. Sun shade retainer

torque increased to 2 in.-lb when the spring was rotated 150 deg to fix the shade in the stowed position. Each of four shade support tubes to which the shade was attached was allowed to deploy independently by the relaxation of a dacron release lanyard attached through a series of eyelets to the solar panel in that bay. The design is shown in Fig. 12. The sun shade was deployed at a rate limited by the solar panel deployment. Full deployment of the shade occurred when the solar panel was three-quarters deployed. The shirt-tail release occurred during the shade deployment when the shade perimeter cord tightened between the two adjacent support tubes. Full deployment was achieved when the perimeter dacron cord was taut.

- (3) *Release lanyard.* The release lanyard was multifilament untreated dacron cord with a breaking strength of approximately 20 lb. Before their installation, the lanyards were tested and pre-stretched by applying 14 lb of tension for 1 h at

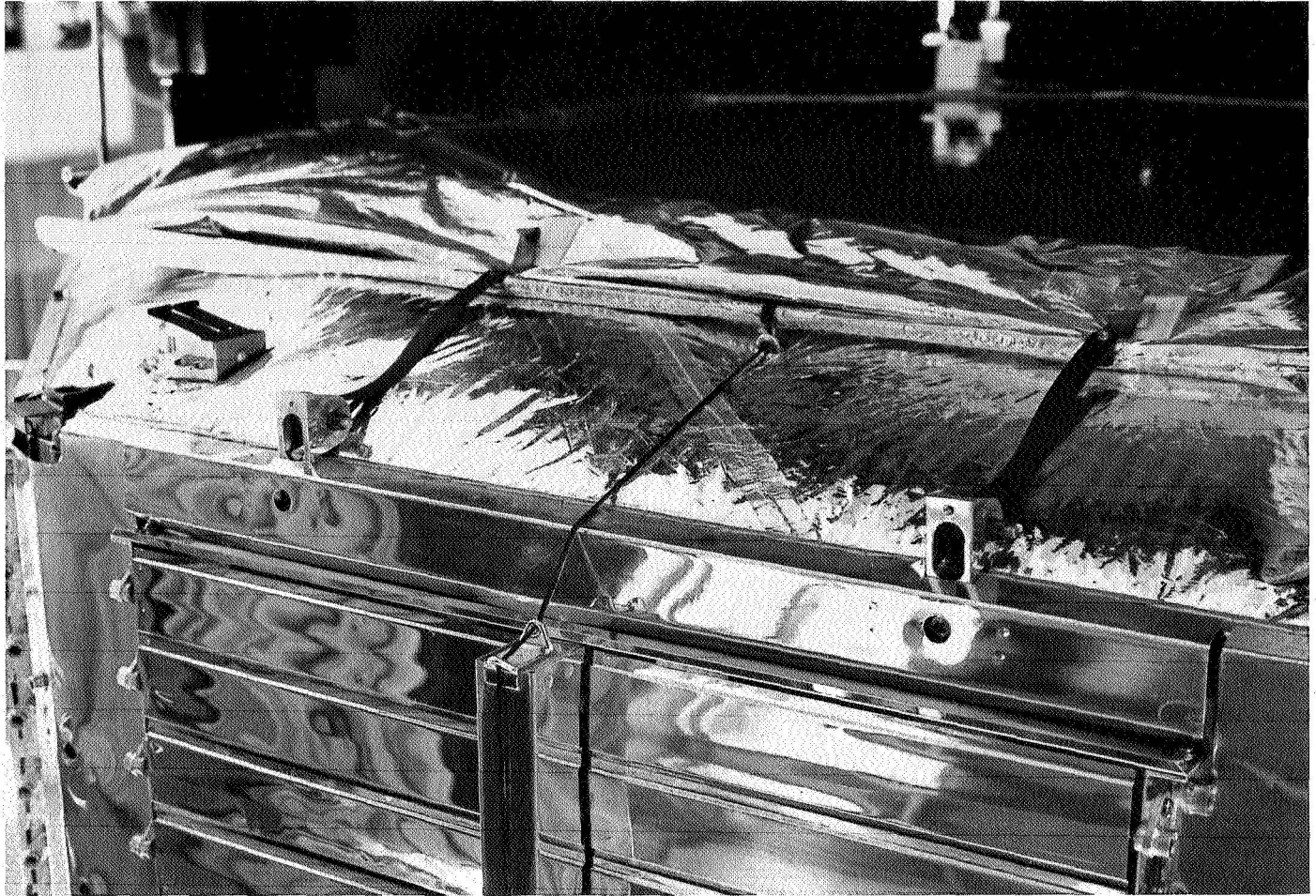


Fig. 12. Sun shade release lanyard

room temperature. The lanyards were then tied to the center of each shade support tube, and the knot was spot-bonded. Each lanyard was routed through three guides, one on the lower ring of the bus and two on the louver housing. Before the lanyard was tied to an eye on the solar panel structure, all twists were removed and the cord was stretched approximately 0.50 in. by pulling it through the eye. The resulting 3.0 lb of preload tension prevented the lanyard from going slack during launch vibration.

E. Attitude Control Jet Shields

Shields were provided to shade the attitude control gas jet assembly at the end of each solar panel. The shield consisted of two parts: (1) a multilayered blanket that contained a clearance hole for the pitch or yaw jet exhausts, and (2) a sheet-metal-blanket support structure which was captured between the solar panel and the

manifold. The blanket was attached to the support by Velcro hook-and-pile strips.

F. Trapped Radiation Detector Shield

This shield, intended for shading the instrument detectors, was similar to the attitude control jet shields. The shield-support structure was polished aluminum sheet metal with the multilayered thermal shield attached to the sunward side and the support attached directly to the instrument mounting brackets.

G. Magnetometer Shield

A multilayered shield with stable thermal properties was required to protect the magnetometer Helmholtz coils. The vacuum-deposited aluminum on the spherical cover had degraded, and the resultant uncertainty in emittance was unacceptable. The shield was constructed of nine layers of aluminized Mylar and faced with

aluminized Teflon, and was attached to the sphere by two draw strings.

H. Surface Coatings and Treatments

Surface coatings and treatments used on the spacecraft are listed in Table 2. These treatments and materials were not exotic. Every effort was made to keep white paint out of the sun to avoid the effects of the uncertainties and degradation in absorptance which characterize these paints. The aluminized Teflon used for the shields and sun shade provided an initial absorptance-to-emittance ratio of 0.244, which was low enough to maintain acceptably cool temperatures for the Mylar shields beneath it.

I. Temperature Control References

The temperature control reference (TCR) assemblies, one mounted at the tip of each of three solar panels, can be seen in Fig. 2. A platinum resistance element was encapsulated in each assembly to measure the temperature from which the solar intensity times the sample absorptance-to-emittance ratio ($S \alpha/\epsilon$) could be deduced. The coatings selected for the sunlit surfaces were

- (1) Cat-A-Lac flat black epoxy paint. A widely used spacecraft coating with well established properties.
- (2) S-13 white. ZnO silicone white paint, a coating frequently used for low α/ϵ applications even though degradation is relatively high.

- (3) S-13M. An experimental white similar to S-13, but formulated with treated ZnO pigment for improved stability.

The TCR design, development, and flight results are given in detail in Ref. 9.

J. Thermal Shield Containers

Because of the problems experienced with the shipping containers for the *Mariner* Mars 1964 spacecraft, new thermal-blanket shipping containers were designed for *Mariner* Venus 67. The *Mariner* Mars 1964 plywood containers and thermal shield protective packing resulted in minor damage, excessive inspection time, static charge buildup, and inadequate cleanliness. For *Mariner* Mars 1964 polished aluminum shields were wrapped in white flannel, and the thermal shield blankets were packaged in plastic bags inside the containers. Unfortunately, the flannel caused an excessive amount of lint, and the plastic bags contributed to a static charge buildup in the blankets.

The new containers for the *Mariner* Venus 67 program were all aluminum with an air-tight closure. Polyurethane foam, configured to fit the hardware and bonded in the containers made additional wrapping unnecessary for the polished aluminum shields. The thermal shield blankets were packaged in lint-free cotton-and-linen bags before being installed in the foam-filled containers.

Table 2. Temperature control surfaces

Assembly	Surface coating or treatment	Nominal properties	
		Solar absorptance	Emittance
Electronic bays under louvers	PV-100 white paint	0.20	0.85
Internal electronic modules (magnesium)	DOW-7	—	0.70
Louver assemblies and side shields	Polished aluminum	0.20	0.05
High gain antenna	Laminar X-500 green paint	0.70	0.85
Omni-directional antenna	Polished aluminum	0.20	0.05
Sunlit solar panel spars	Polished aluminum	0.20	0.05
Shaded solar panel structure	Cat-A-Lac flat black epoxy paint	0.95	0.85
Magnetometer	Polished aluminum and PV-100 white paint	0.20	0.05
		0.20	0.85
Plasma probe	Sunlit surface gold-plated; sides S-13 white paint	0.25	0.04
		0.20	0.85
Sun sensor pedestals	S-13 white paint	0.20	0.85
Shields and sun shade	1-mil FEP Teflon aluminized on back side	0.13	0.55

V. Test Program

Besides full-scale space simulator tests, which will be described, a series of developmental, qualification, and acceptance tests were performed that are described in detail in Ref. 10. Individual thermal tests were carried out for the TCRs, magnetometer sensor, and solar panel end fittings (monoballs). Two series of comparison-calibration tests of radiometers used in the space simulator were conducted. The thermal shields and sun shades were subjected to a complete series of qualification (type approval) and flight acceptance tests. In addition to the flight vibration and space simulator tests on *Mariners 67-1* and *67-2*, the hardware was qualified during the structural test model (STM) vibration tests, and temperature control model (TCM) space simulator tests. The blanket tests included launch pressure profile tests in a vacuum chamber. The deployable sun shade was subjected to a series of deployment tests on the TCM, STM, and flight spacecraft, a long-term storage test, adapter hang up tests (effect of a lanyard failure before separation of the spacecraft from the booster), and stray light reflectance tests.

Major milestones of the project are tabulated here, followed by descriptions of space simulator tests.

Schedule summary	
Project initiation	1965 – December 22
TCM test	1966 – June 24 to July 6
M67-1 test	1967 – January 13 to 27
M67-2 test	– March 22 to April 4
M67-1 Cape shipment	– April 20
M67-2 Cape shipment	– April 27
Launch	– June 14

A. Temperature Control Model

The TCM tests, conducted in the JPL 10-ft space simulator, were made to verify the adequacy of the basic thermal design, to empirically establish detailed thermal design features, and to empirically establish the influence of various thermal parameters on spacecraft temperatures. Some results are summarized in Table 3. The thermal characteristics of the space simulator are given in Ref. 11. Figure 13 shows the TCM suspended in the simulator.

The TCM was a full-scale mockup of the flight spacecraft assembled from flight-type structural and mechani-

Table 3. Summary of test data (°F) for M67-1

Location	TCM earth cruise	M67-1		
		Earth cruise before change	Earth cruise after change	Postplayback cruise, after change
Bay 1	64	56	62	84
2	48	42	46	69
3	64	55	59	74
4	61	52	56	76
5	56	50	54	70
6	64	54	60	79
7	58	53	61	76
8	67.5	64	66.5	82
Bus Average	60	53	58	76

cal parts. Mockups were made if flight parts were not available. External design and surface preparation duplicated the flight spacecraft design at the time the TCM was built. The TCM contained no electronics. Power dissipation was simulated by appropriately placed electrical heaters. The power values used were obtained directly from cognizant engineers of the electronics. Owing to size limitations of the solar beam and space simulator, special electrically heated solar panel mockups were used in place of real panels.

The test series was performed in three parts. Part 1 established that the temperature control provisions were adequate for the coolest and warmest modes during the primary mission. An additional mode at 285 W/ft² was performed because intensity monitoring radiometers disagreed. Minor changes to the trapped radiation detector (TRD) and magnetometer were made at the end of part 1.

During part 2, solar intensity, internal power, and solar panel temperatures were varied to enable an evaluation of their influence on spacecraft temperatures. Two *temperature matching* modes were particularly significant. With solar simulation lights turned off, heater power was increased until temperatures were reached that were identical to two previous modes with lights on. The increase in internal power was then equal to the solar heating for the earlier modes. Solar heating of the bus was thus established as 18.5 W at earth and 36 W at Venus, excluding inputs from the solar panels and sun sensors. Minor modifications to the trapped radiation detector and magnetometer were again made at the end of part 2.



Fig. 13. TCM in JPL 10-ft space simulator

In part 3, two modes were run with the sunshade in the stowed position. The temperatures obtained represent a worst-case failure of the shade to deploy; that is, all four of the independent motions failed. During this test, both the mean temperature and the earth-to-Venus temperature-rise increased significantly.

B. Flight Spacecraft

1. *The M67-1.* The flight-support spacecraft M67-1 was tested in the JPL 10-ft space simulator. The simulator test was run in two parts: a system test (part 1) and a thermal test (part 2). The primary objective for part 2 was to verify the capability of the temperature control subsystem to maintain spacecraft temperatures within allowable bounds in a flight environment. Significant test results are summarized in Table 3.

a. *Bus modification.* The biggest surprise of the test was the discrepancy of 7°F in average bus temperature between the M67-1 and the TCM for the earth cruise mode. The lower M67-1 temperature was caused by a difference in power dissipation of about 10%. This power discrepancy was noted during part 1, but it was decided that maximum thermal information would be obtained by making any required changes during part 2. There was also some question as to the accuracy of the telemetry-derived power measurement. A historical summary of the various values of bus-dissipated power for earth cruise, cavity amplifier, and battery charger *off* is as follows:

Power, W	Source	Date
158	Temperature control personnel (for TCM)	1966-June
153	Design Specification	-November
151	SAF measurement	-December
141	Spacecraft telemetry (channel 447)	1967-January
142	SAF measurement	-February

The post-test SAF (Spacecraft Assembly Facility at JPL) measurement confirmed that the TCM power level for this mode was high by 16 to 17 W.

Although the 7°F drop in bus temperature still left a margin of about 15°F before the spacecraft would be endangered by a freezing of the PIPS propellant, about

half of the 30 W cold-end thermal margin had disappeared. Louvers, which open at 55° to 60°F, were nearly all closed, and the spacecraft was considered to be unnecessarily close to freezing.

Of additional concern was the limited capability to increase bus temperatures without major redesign. The bus depended on internally dissipated power to maintain acceptable temperatures, because it had been shielded from solar heating. If this power is insufficient, two choices exist:

- (1) Radiating surfaces can be shielded to impede heat loss.
- (2) Sunlight can be allowed to enter.

Option 2 was clearly undesirable, but only about 0.5 sq ft of unshielded radiating area was available. Calculations indicated that this area was just sufficient to return bus temperatures to TCM levels, but necessary idealizations made these calculations optimistic. An early determination of the adequacy of this change was required, so the test was interrupted during part 2. Modifications effected are as follows:

- (1) Added bottom case shields on bays 1, 3, 5, 7, and 8. Area of covered white paint = 47.5 in².
- (2) Added top case shields on bays 1 and 6. Area of covered white paint = 37.8 in².
- (3) Added superinsulation boot to upper shield at superstructure in corner D. Area of covered opening = 7 in².

The resultant configuration of side shielding can be seen in Fig. 6. These modifications produced the desired effect, raising the average bus temperature 5°F. Owing to limited time, the revised thermal design was checked for only the coldest and hottest mission modes. Ample margin existed for both cases.

b. *Steady-state considerations.* Previous experience with *Mariner* spacecraft indicated that steady-state was always reached within 12 h and, for minor mode changes, was usually achieved within 4 to 6 h. These neat *rules-of-thumb* were disproved during the part 2 tests. The first mode of this series was the cold-end earth cruise mode. After 12 h of this mode, a drop in bus temperatures of about 1°F in the preceding 2 h was interpreted to mean that, for all practical purposes, steady-state had been achieved. The solar intensity was lowered to 100 W/ft² and the spacecraft remained in this mode for an additional 12 h. At the completion of this mode, the

battery charger was turned on and the solar intensity was increased to 126 W/ft². It became obvious after about 6 h that, even with the additional power dissipation from the battery charger, spacecraft temperatures would not rise to the levels of the first mode of the series. The spacecraft had clearly not reached steady-state in the first mode. The battery charger was turned off and the first mode repeated, this time for 24 h. A comparison of data showed that the bus was about 5°F from steady-state in the first mode.

The reason for the unexpected behavior of the bus is apparent in retrospect. The louvers were virtually all closed, and this magnified the temperature effect of the nonequilibrium condition. Had the bus temperature been within the louver range, the rate of temperature change would have indicated that steady-state was less than 2°F away. The lesson, relearned, was that general rules for steady-state determination must be used with caution.

c. Operational support equipment effects. Overall bus temperatures were little affected by OSE cabling, light hoods, and other support equipment. Except for directly affected components, such as sun sensors, part 1 temperature data can be used without major correction. This data is particularly valuable in deducing the effect on spacecraft temperatures of various parametric changes. For this reason, the elimination of several modes during part 2 did not seriously affect the test value from a temperature control point of view.

2. The M67-2. The M67-2 flight spacecraft underwent system tests in the JPL 10-ft space simulator similar to those performed with M67-1.

Significant thermal test results are given below in Table 4.

The earth cruise mode shown was for minimum spacecraft power; the postplayback mode had near-maximum power dissipation.¹ The M67-1 and M67-2 earth cruise modes were comparable except for a 10% lowering of intensity for cold margin checking of M67-2. This intensity difference and a data encoder temperature reference shift on M67-1 account for about 2° of the 4.5°F difference in average bus temperature. The remaining 2.5°F was within the expected spacecraft-to-spacecraft variation in thermal characteristics.

¹Earth cruise: cavity amplifier on, battery charger off.

Postplayback cruise: travelling wave tube on, battery charger off, gyros on, tape electronics on.

Table 4. Summary of test data (°F) for M67-2

Location	M67-1	M67-2	
	Earth cruise 126 W/ft ² (after modifications)	Earth cruise 112 W/ft ²	Postplayback cruise 290 W/ft ²
Bay 1	62	58	75
2	46	41	65
3	59	54	72
4	56	52	74
5	54	51	72
6	60	55	78
7	61	54	70
8	66.5	64	76
Bus Average	58	53.5	73

This test, together with the corresponding M67-1 test, permitted the following conclusions to be made:

- (1) The thermal design was judged adequate for all anticipated combinations of spacecraft operating mode and flight environment.
- (2) All flight telemetry temperatures were within design accuracy.
- (3) OSE installed in the simulator during the system portion of the test (part 1) had only a minor influence on bus temperature.
- (4) Discrepancies of 6% to 12% still existed between the various intensity monitors used, though this disagreement was less for M67-2 than that observed during the M67-1 test.
- (5) M67-2 had thermal characteristics similar to M67-1.

VI. Analysis

The relative emphasis given tests and analyses on this program was somewhat different than is usual for earth satellites. In the latter case, a detailed computer model is derived for use in thermal design. The resulting spacecraft design is tested under known boundary conditions, and the computer model is revised to more accurately represent the internal thermal characteristics of the spacecraft. The updated model is then used for the prediction of flight temperature profiles. For *Mariner Venus 67*, a fairly coarse computer model was generated early in the program for design use. The resulting design was verified — and modified as necessary — during space

simulator testing of the temperature control model. In addition, thermal transfer functions were empirically established. The computer model was revised for predicting flight temperatures for those situations which could not be simulated (i.e., launch, midcourse, encounter). Cruise temperature predictions and detailed modifications to the thermal design were based on space simulator test data, corrected for known test errors. The 1967 philosophy, then, was to use test data whenever possible for both design purposes and flight predictions because of its superior correlation with flight data. This result is in turn the effect of rather good facilities for the simulation of the simple boundary conditions during ordinary sun-oriented cruise. Analysis was still essential for the other purposes outlined, but the time and money expended for tests far exceeded these efforts.

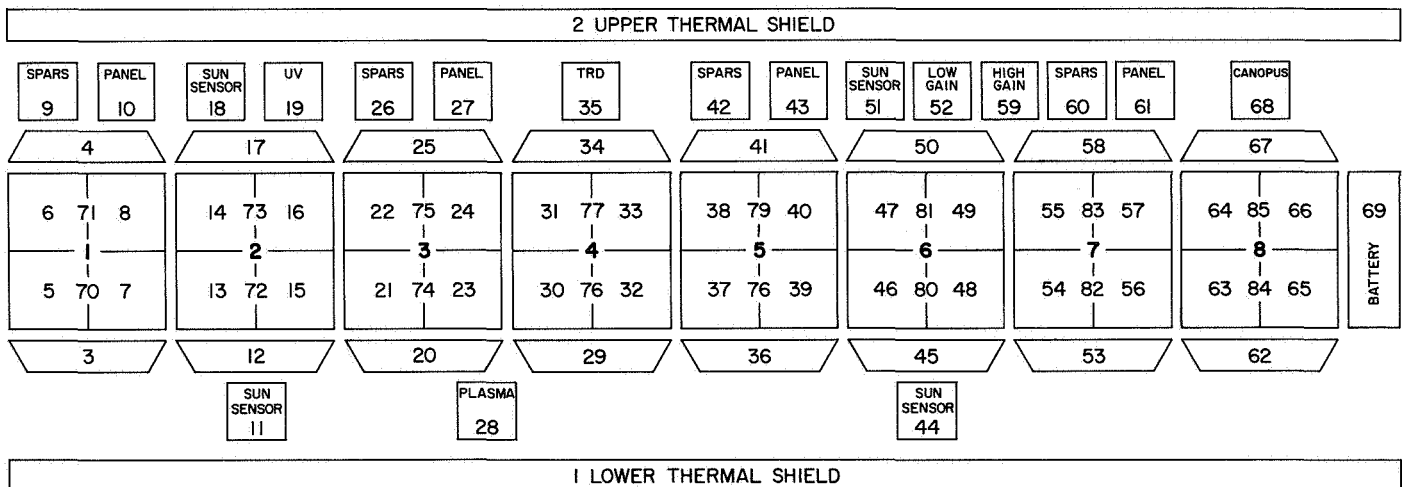
Figure 14 is a schematic representation of the nodal model of the spacecraft. Each bay was divided into quadrants. Separate dummy nodes (70 to 85) were used to obtain the average temperature of adjacent quadrants to *actuate* the louvers shared by these quadrants. Internal tankage was not simulated. Instead, each quadrant was assumed to have a view factor of 1.0 to the nearest thermal shield, either upper or lower. This artifice had the effect of providing *one-stop* radiation resistance between any quadrant and the rest of the bus on the same

level, again either upper or lower. Radiant heat transfer between the upper and lower bus was provided by a radiation link between upper and lower shields. These approximations have some obvious shortcomings, but because gradients within the bus are fairly small ($<30^{\circ}\text{F}$) the resultant errors are not too serious.

The computer program used was the transient version of the HAC TAP (Hughes Aircraft Company Thermal Analyzer Program), modified to permit emittance dependence on temperatures (louver capability). The analysis produced fairly good results for bus temperatures, but the model was too coarse to yield good data for appendages. For instance, because the conduction tie of sun sensors with the octagonal ring structures was not well represented by a single term some supplementary analyses were required.

VII. Flight Results

Mariner V flight telemetry included measurements from 37 platinum wire resistance thermometers. Appendix B shows the construction of the transducer used and its locations on the spacecraft. The voltage drop across the platinum resistor was measured with 1 mA constant-current input. Each transducer was sampled at an interval ranging from 14 min to 2 h 48 min, depending on the



NOTES

- THIS IS VIEW AS SEEN FROM INSIDE SPACECRAFT.
- NODES 70-85 ARE LOUVER ACTUATOR NODES.
- NODES 4, 17, 25, ETC. ARE UPPER RING SECTIONS.
- NODES 3, 12, 20, ETC. ARE LOWER RING SECTIONS.

Fig. 14. Analytical nodal network

Table 5. Telemetered flight temperatures (°F), predicted and actual

Telemetry channel	Location	Pre-Canopus acquisition ^a		Earth cruise ^b		Venus cruise ^c	
		Predicted	Actual	Predicted	Actual	Predicted	Actual
401	Bay 1	72	74	68	68	65	67
421	Bay 2	50	53	45	47	55	57
402	Bay 3	62	64	57	59	67	69
422	Plasma probe	105	105	105	105	196	214
403	I _{sc} - V _{oc} transducer	127	104	127	104	239	226
423	Bay 4	59	63	54	56	68	70
404	Bay 5	58	60	52	53	66	68
424	Voltage controlled oscillator	64	66	59	59	74	76
405	Bay 6	62	63	57	57	72	75
425	-Y pitch jet assembly	-30	-15	-30	-12	52	53
406	+X roll and yaw jet assembly	-30	-25	-30	-25	52	44
426	Bay 7	63	63	54	54	60	60
407	Bay 8	91	95	86	85	83	83
427	Solar panel 5 spar	43	85	43	93	140	132
408	PIPS N ₂ tank	57	60	51	52	60	62
428	Battery	71	71	64	62	65	65
409	Solar panel 4A1	127	119	127	119	239	240
429	Solar panel 4A5	127	116	127	118	239	239
410	Canopus sensor	64	65	59	57	61	61
430	Primary sun sensor	52	54	47	49	78	101
431	Low-gain antenna mast	-105	-90	-105	-90	-95	-83
412	TCR S13	Off scale	Off scale	-25	-29	Off scale	Off scale
432	TCR S13M	-55	-52	-55	-48	Off scale	Off scale
413	TCR black	149	140	149	138	Off scale	Off scale
433	-X roll and yaw jet assembly	-30	-25	-30	-24	52	46
414	Auxiliary oscillator 1	68	70	62	62	73	74
434	Upper thermal shield	-192	-194	-192	-197	-142	-170
435	Lower thermal shield	45	35	45	37	132	167
436	Tape recorder	58	61	52	54	66	68
437	UV photometer	52	54	47	46	59	60
418	Auxiliary oscillator 2	68	67	62	62	75	75
438	Trapped radiation detector	48	52	43	45	56	58
419	High-gain antenna	-220	-195	-220	-197	-175	-151
439	Magnetometer	-16	7	-16	7	-25	5
217	Propellant tank	61	65	55	56	64	66
218	+X/-Y N ₂ tank	65	68	58	59	65	66
219	-X/+Y N ₂ tank	61	64	56	57	67	69

^aCavity amplifier on, battery charger on, gyros on.

^bCavity amplifier on, battery charger on, gyros off.

^cTravelling-wave tube on, battery charger off, gyros off.

flight phase. These measurements are considered accurate to within 2°F.

Table 5 lists predictions and actual flight data for cruise conditions near earth and near Venus. Predictions were normally based on space simulator test data, corrected for systematic test errors.

A tabulation of known error sources of tests, with an estimate of their effect on average bus temperature, is given. These estimates are derived from analyses, test observations, experience, and guesswork. The tabulation applies only to the earth cruise, louvers-closed mode which is the mode most sensitive to test errors. The *bias* is the calculated offset in bus temperature caused by this effect; the *uncertainty* is the estimated maximum deviation from the test temperature after correction for the bias. Flight temperature is taken as reference; positive values in the table indicate that the spacecraft is warmer in the chamber than in flight.

Error source	Bias, °F	Uncertainty, °F
Sticky louvers	-1	±1
Measurement inaccuracy	0	±2
Failure to achieve steady-state	-0.5	±0.5
Inaccuracies in solar panel mockups	0	±1
Cabling effects	-3	±1.5
Chamber-heat inputs	+7	±2
Solar intensity	0	±2
Net effect	+2.5	±10

After launch, the earlier predicts were updated to agree with flight data, and expected temperature-time profiles for the mission were generated. The solar intensity at the spacecraft is shown in Fig. 15. The predictions are shown together with flight data in Figs. 16 to 40 and 42 to 49.

A. Launch

Since temperatures were read infrequently during launch and time gaps occurred in data received during the parking orbit, relatively little temperature data are available before the sun was acquired. All the

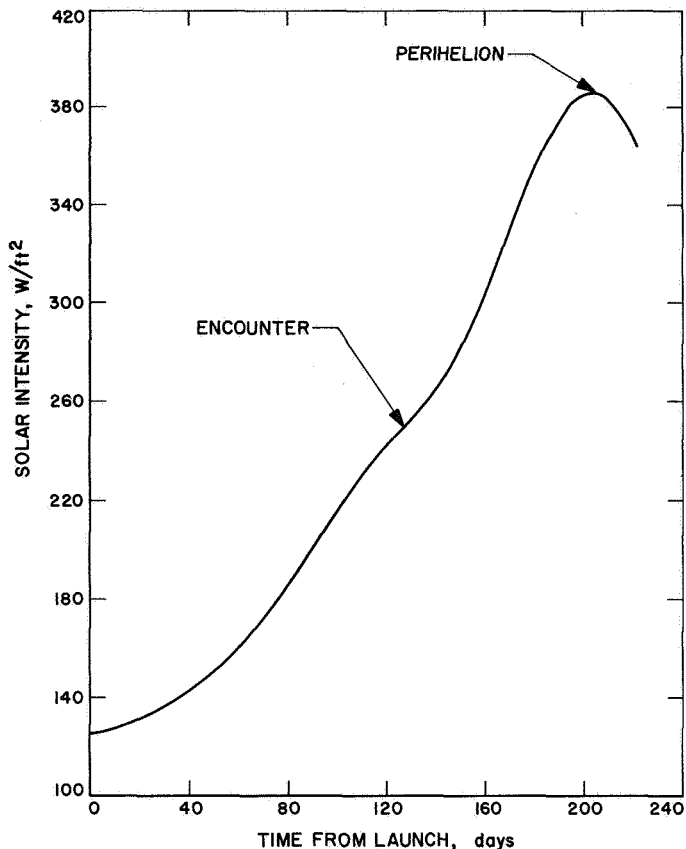


Fig. 15. Solar intensity at Mariner V spacecraft

data observed were entirely normal. Very little temperature change was observed in the bus during ascent and parking orbit. Temperatures at sun acquisition were on the cool side of nominal, but were within expected tolerances. A cooling of external items was caused during boost by the expansion of gas under the shroud; and further cooling occurred while the spacecraft was in the shadow of the earth. No extreme transients were observed, and all spacecraft components remained well within allowable limits.

B. Midcourse Maneuver

Figures 50 through 54 show temperature-time histories of the spacecraft at various transducer locations. The maneuver performed was a 55-deg pitch, 71-deg roll, and 15 s burn, in that order. This maneuver initially turned bay 3 toward the sun; the subsequent roll turned bays 2 and 1 toward the sun. Since prelaunch analysis had shown that worst-case maneuvers would not cause overheating of the spacecraft, no computer analysis of this specific maneuver was made. The data were generally consistent with estimates.

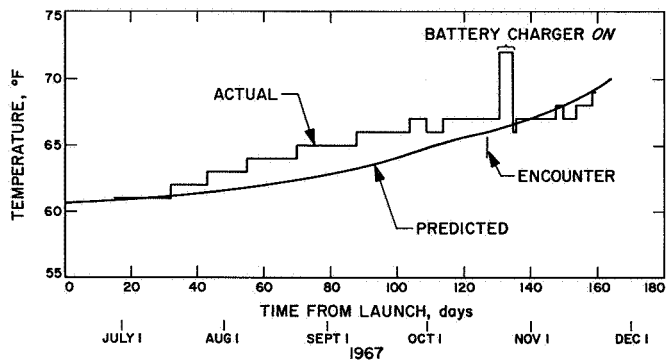


Fig. 16. Bay 1 flight temperature, channel 401

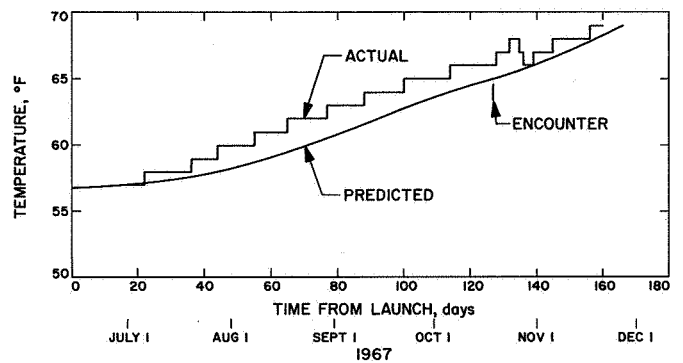


Fig. 19. PIPS propellant tank flight temperature, channel 217

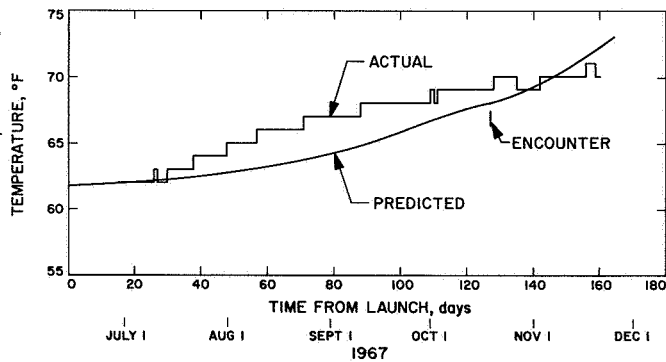


Fig. 17. Bay 3 flight temperature, channel 402

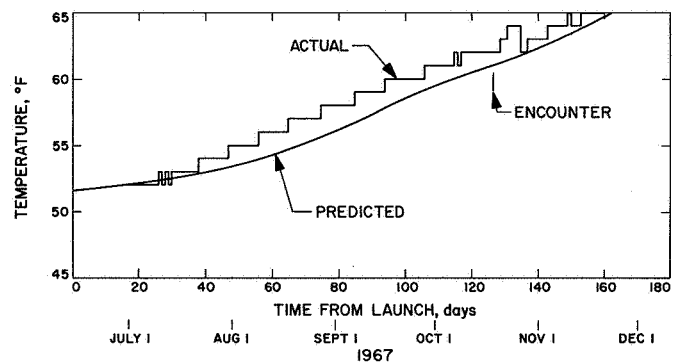


Fig. 20. PIPS N₂ tank flight temperature, channel 408

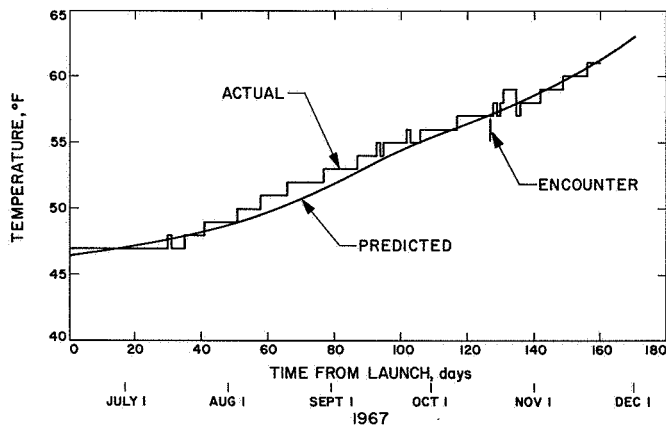


Fig. 18. Bay 2 flight temperature, channel 421

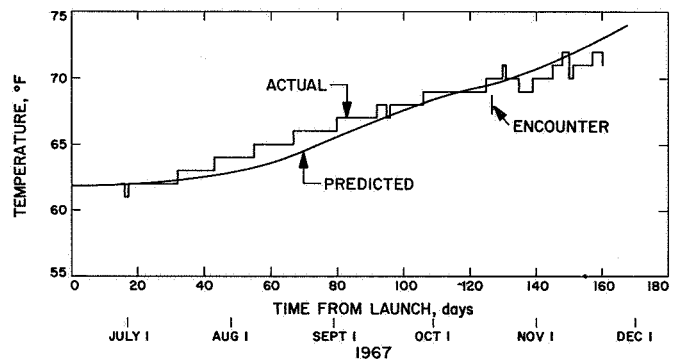


Fig. 21. Bay 4 flight temperature, channel 423

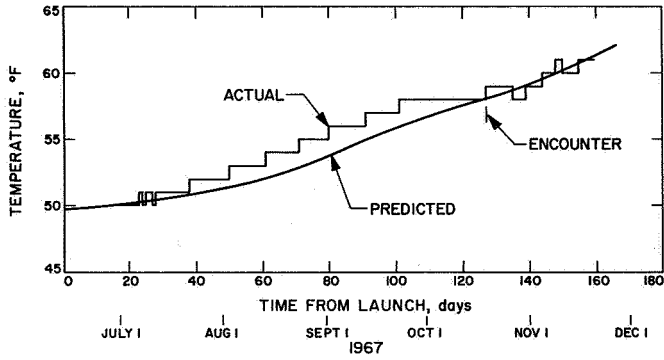


Fig. 22. Trapped radiation detector flight temperature, channel 438

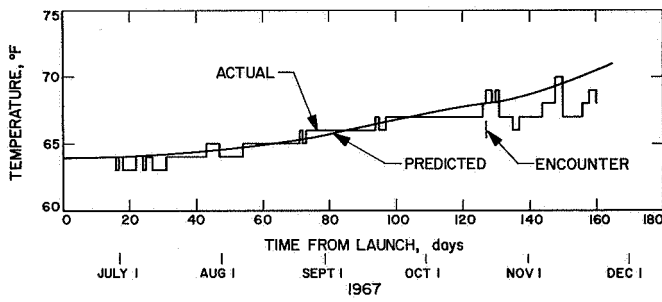


Fig. 23. Bay 5 flight temperature, channel 404

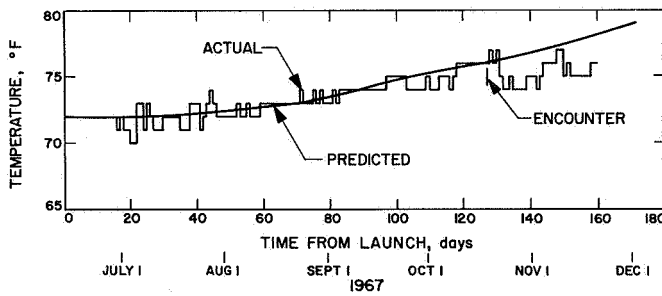


Fig. 24. Voltage controlled oscillator flight temperature, channel 424

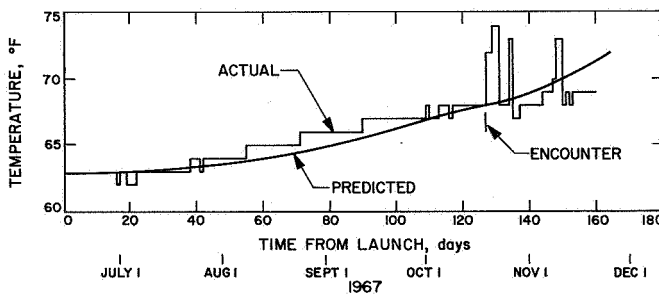


Fig. 25. Tape recorder flight temperature, channel 436

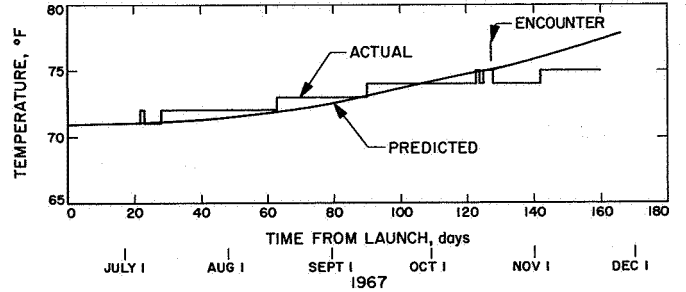


Fig. 26. Bay 6 flight temperature, channel 405

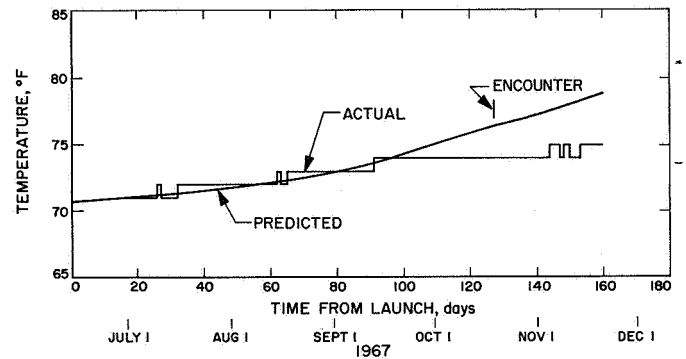


Fig. 27. Auxiliary oscillator 1 flight temperature, channel 414

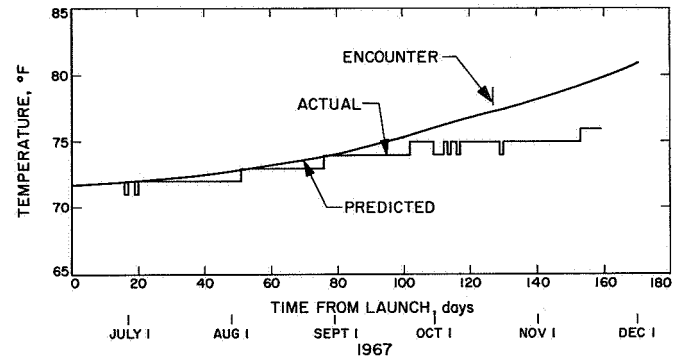


Fig. 28. Auxiliary oscillator 2 flight temperature, channel 418

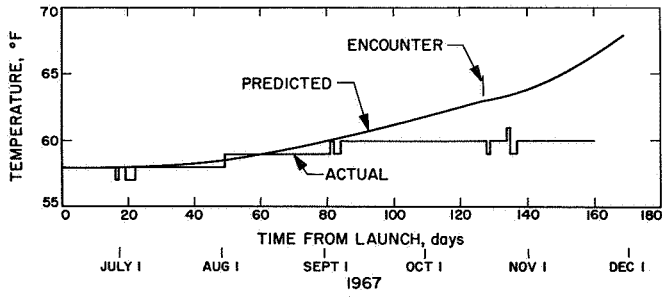


Fig. 29. Bay 7 flight temperature, channel 426

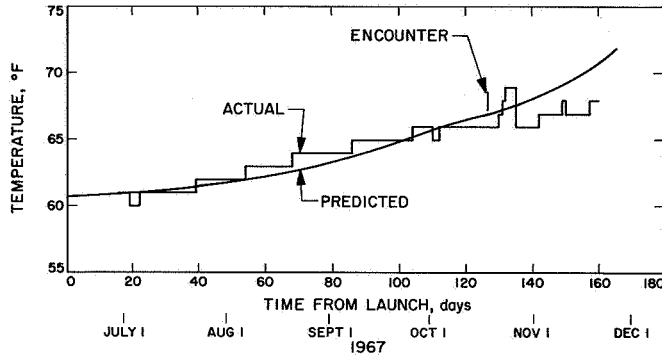


Fig. 30. +X/-Y attitude control N₂ tank flight temperature, channel 218

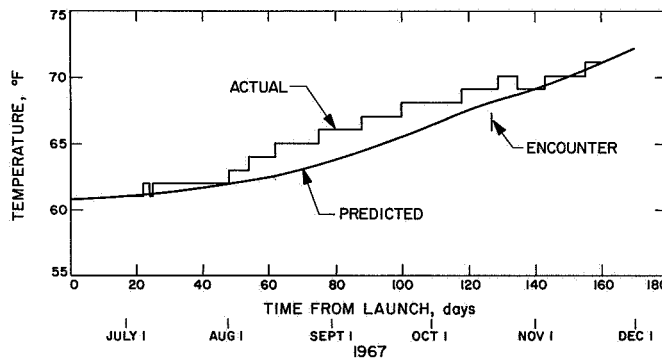


Fig. 31. -X/+Y attitude control N₂ tank flight temperature, channel 219

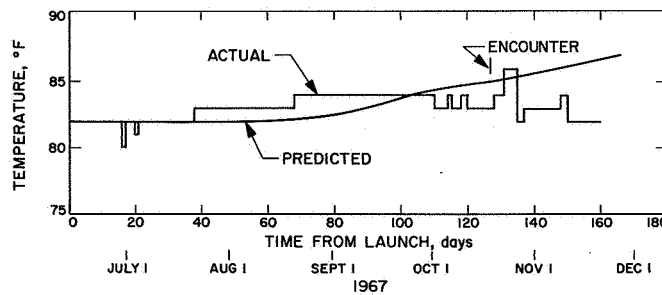


Fig. 32. Bay 8 flight temperature, channel 407

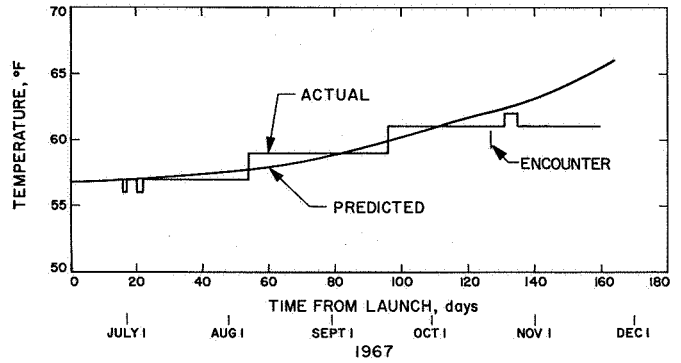


Fig. 33. Canopus sensor flight temperature, channel 410

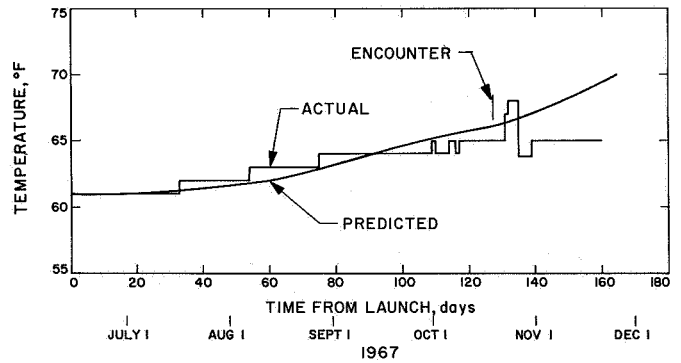


Fig. 34. Battery flight temperature, channel 428

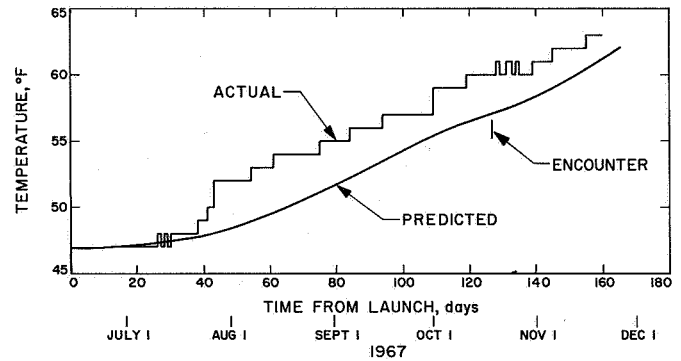


Fig. 35. UV photometer flight temperature, channel 437

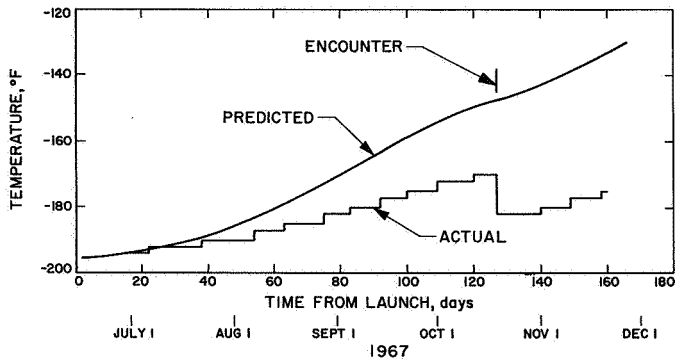


Fig. 36. Upper thermal shield flight temperature, channel 434

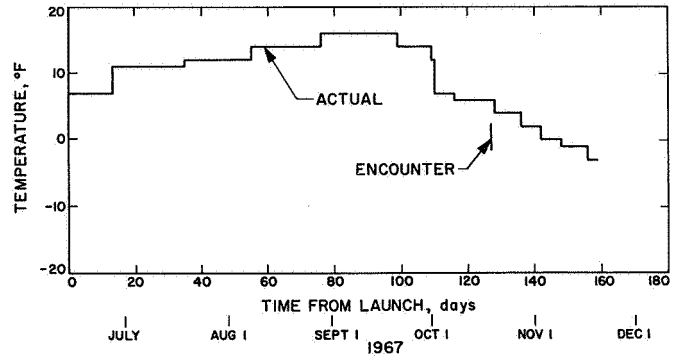


Fig. 39. Magnetometer flight temperature, channel 439

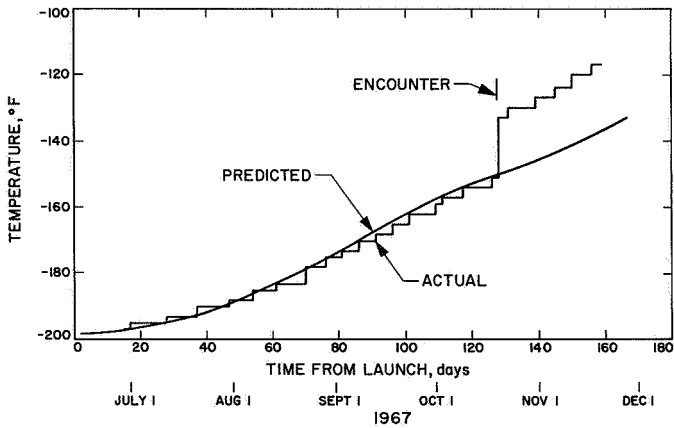


Fig. 37. High gain antenna flight temperature, channel 419

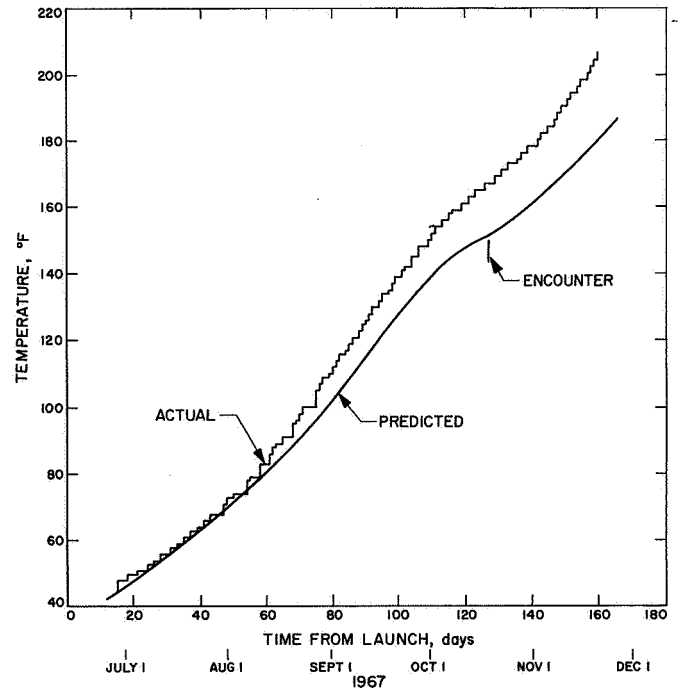


Fig. 40. Lower thermal shield flight temperature, channel 435

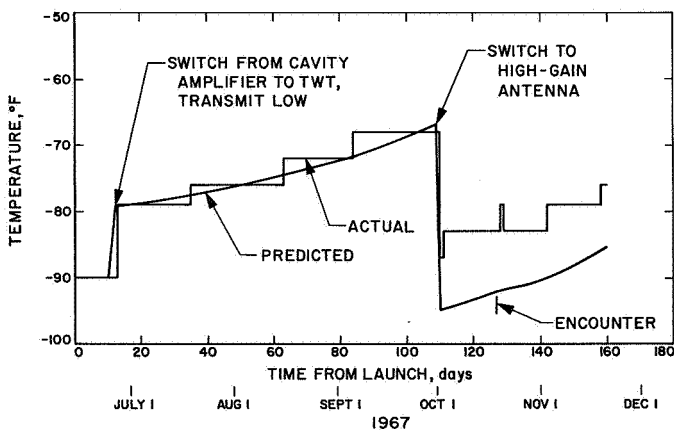


Fig. 38. Low gain antenna mast flight temperature, channel 431

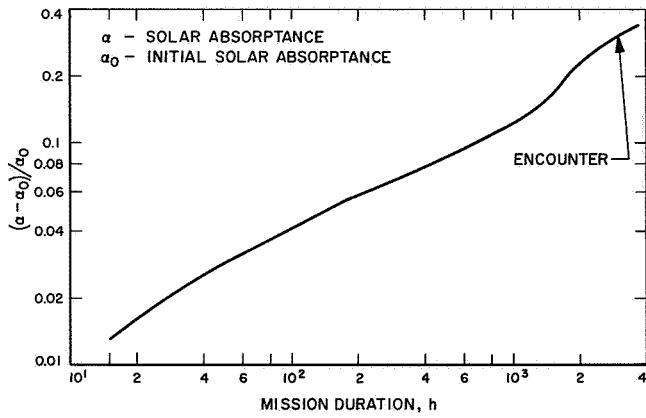


Fig. 41. Lower thermal shield degradation

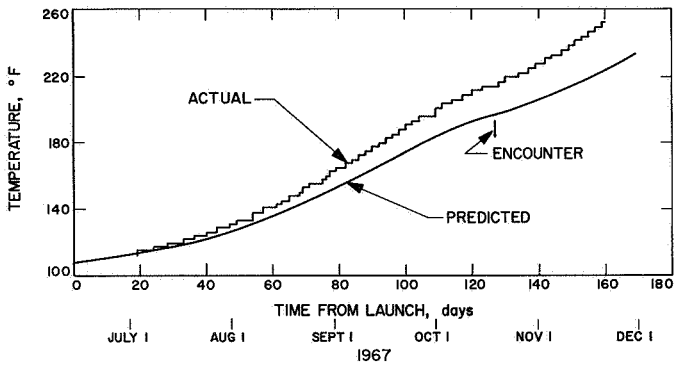


Fig. 42. Plasma probe flight temperature, channel 422

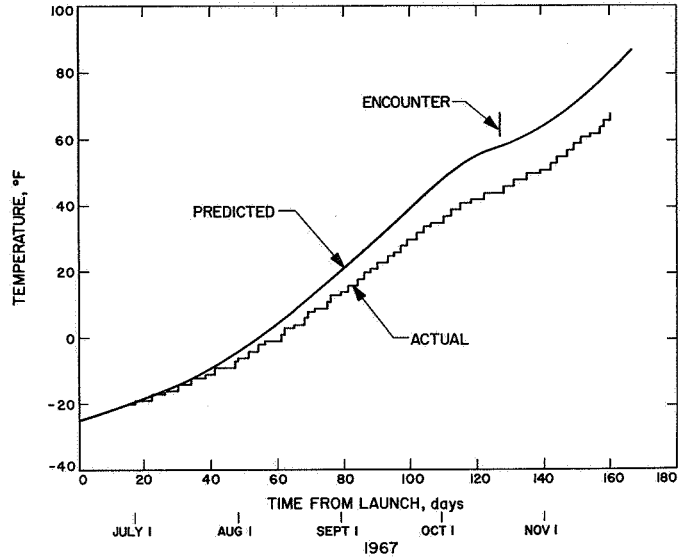
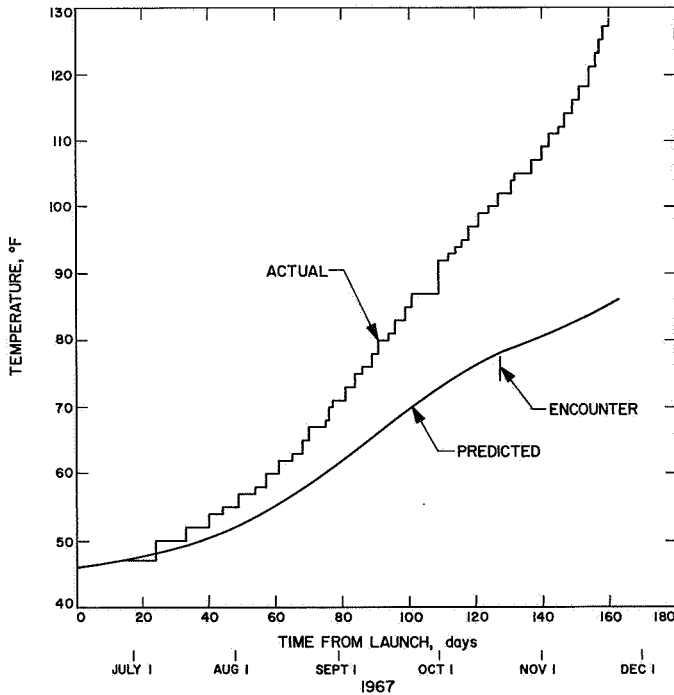


Fig. 44. +X roll and yaw jet assembly flight temperature, channel 406

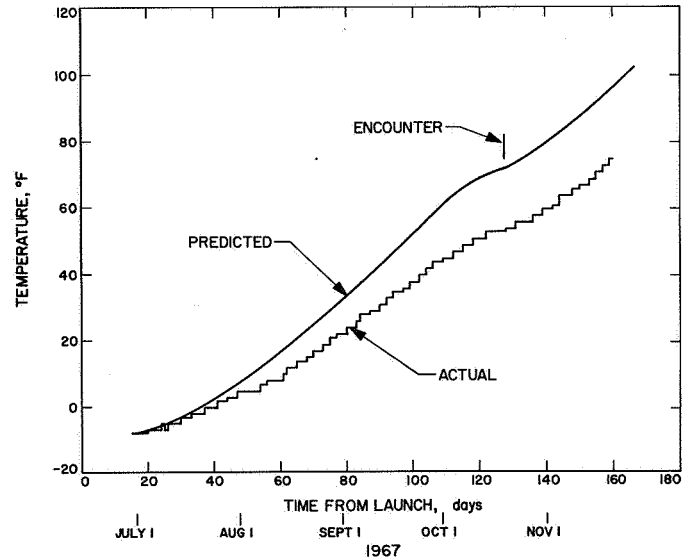


Fig. 45. -Y pitch jet assembly flight temperature, channel 425

Fig. 43. Primary sun sensor flight temperature, channel 430

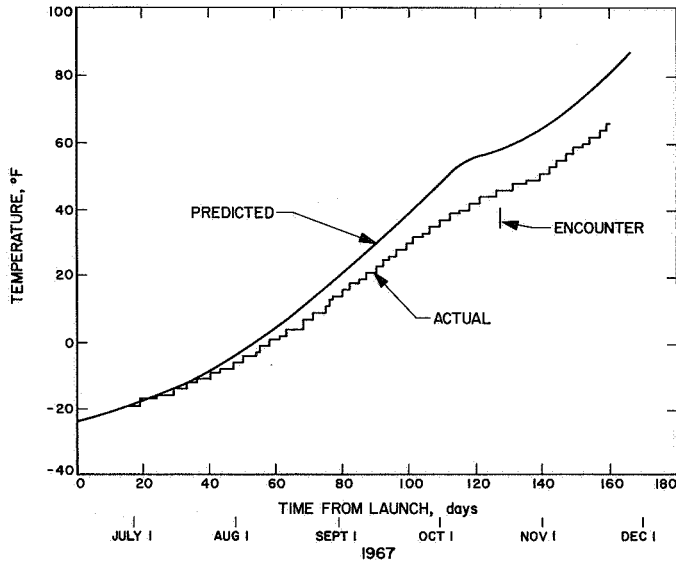


Fig. 46. -X roll and yaw jet assembly flight temperature, channel 433

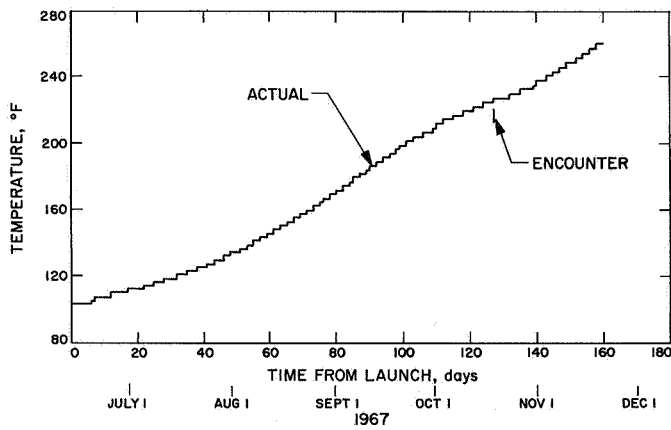


Fig. 47. $I_{sc} - V_{oc}$ solar cell flight temperature, channel 403

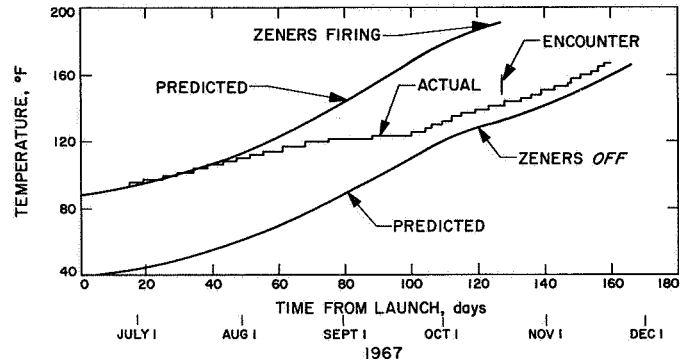


Fig. 48. Solar panel spar flight temperature, channel 427

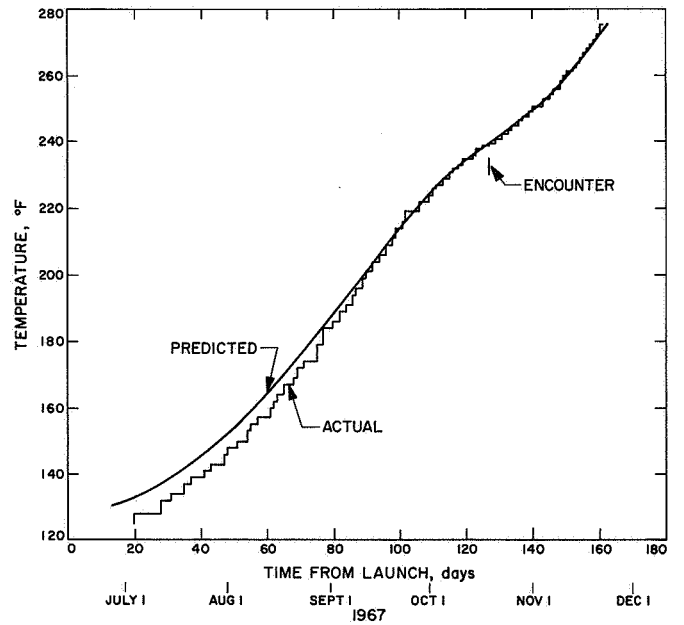


Fig. 49. Solar panel flight temperatures, channels 409 and 429

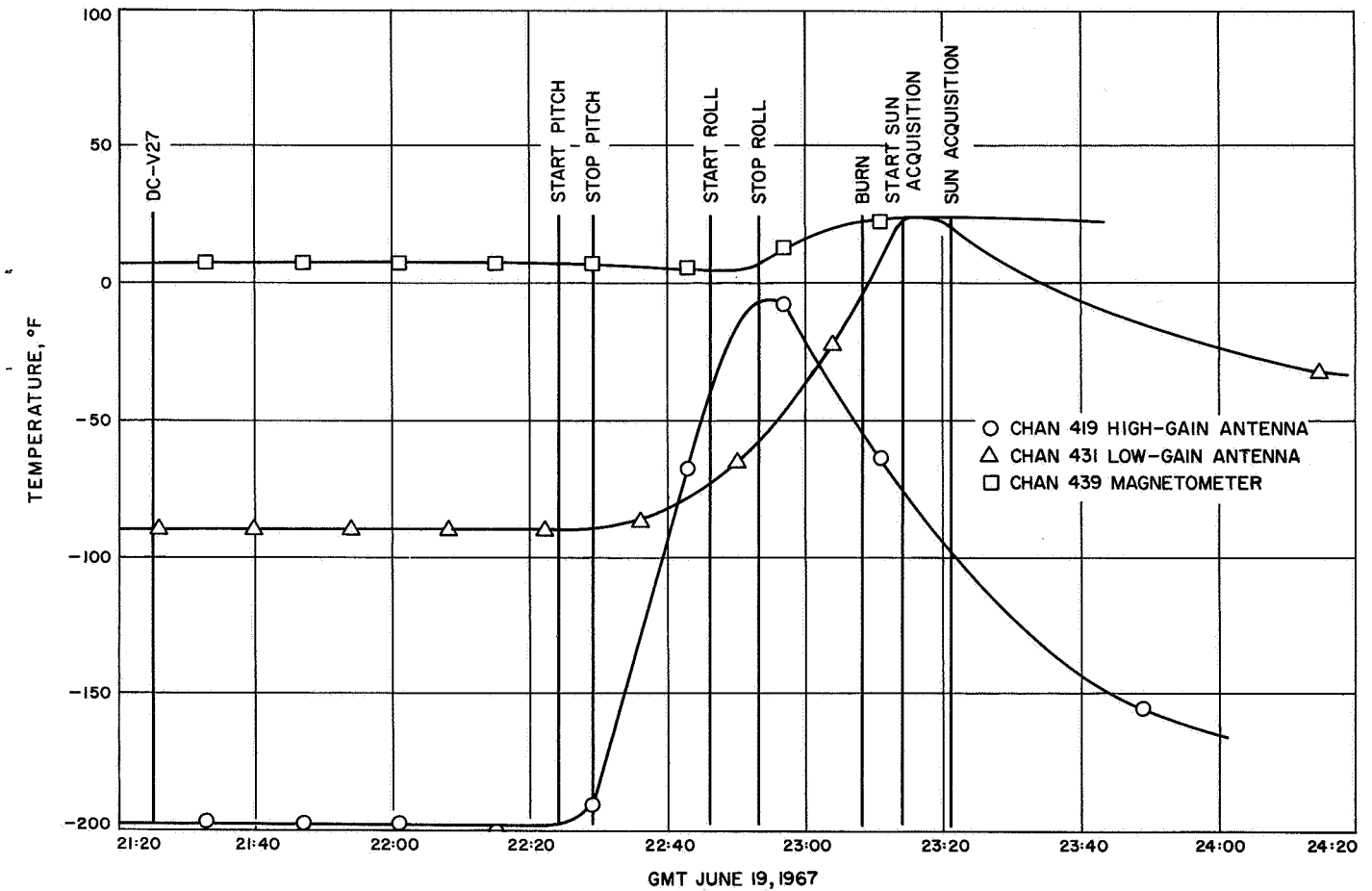


Fig. 50. Midcourse transient temperatures for antennas and magnetometer

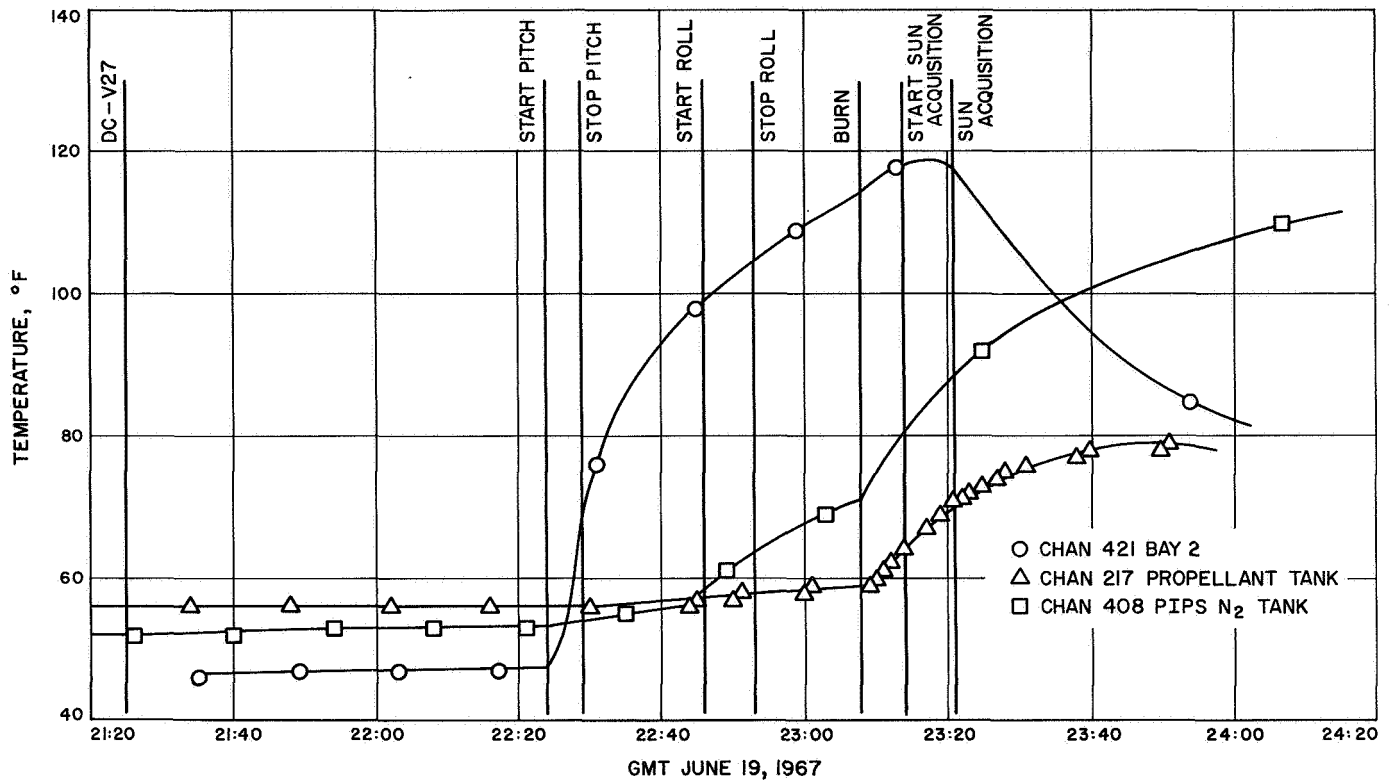


Fig. 51. Midcourse transient temperatures for propulsion subsystem

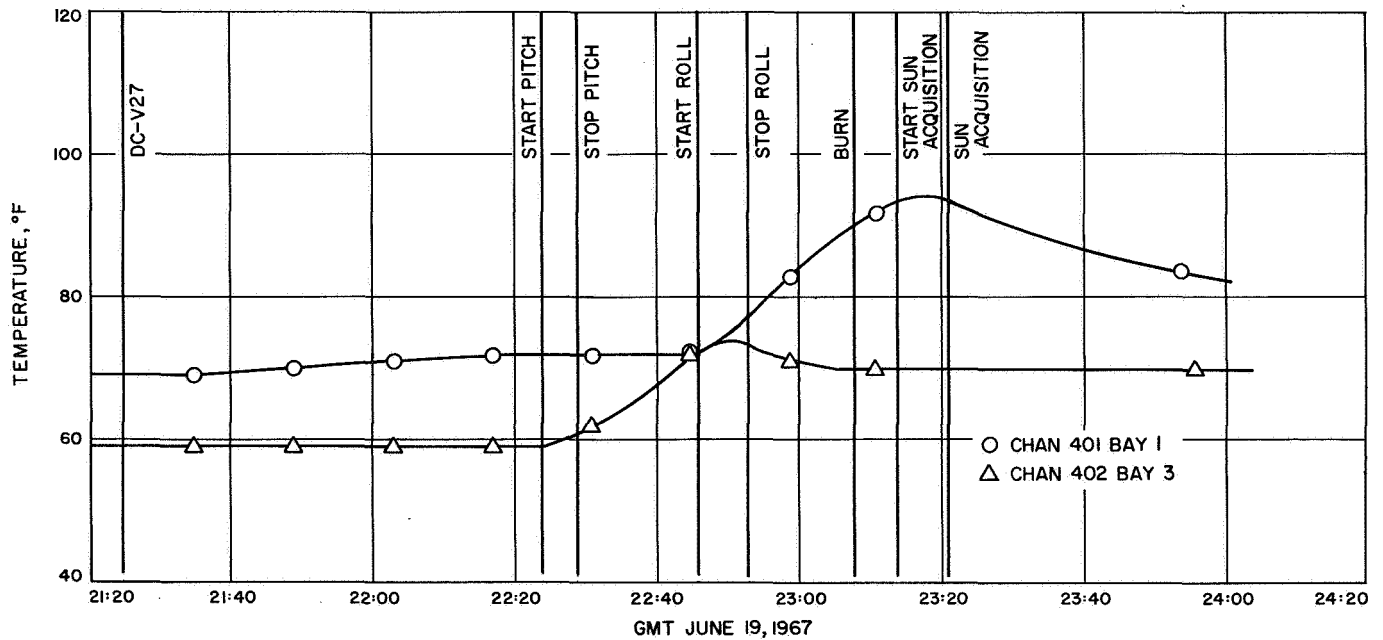


Fig. 52. Midcourse transient temperatures for bays 1 and 3

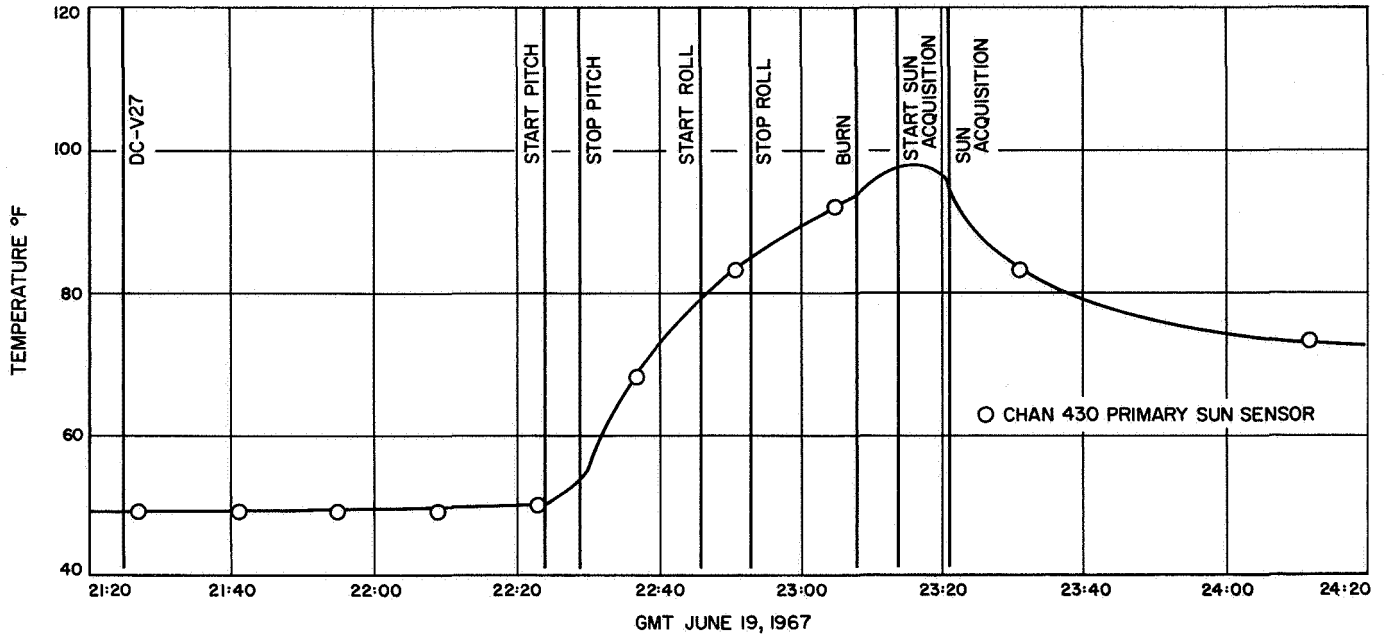


Fig. 53. Midcourse transient temperatures for primary sun sensor

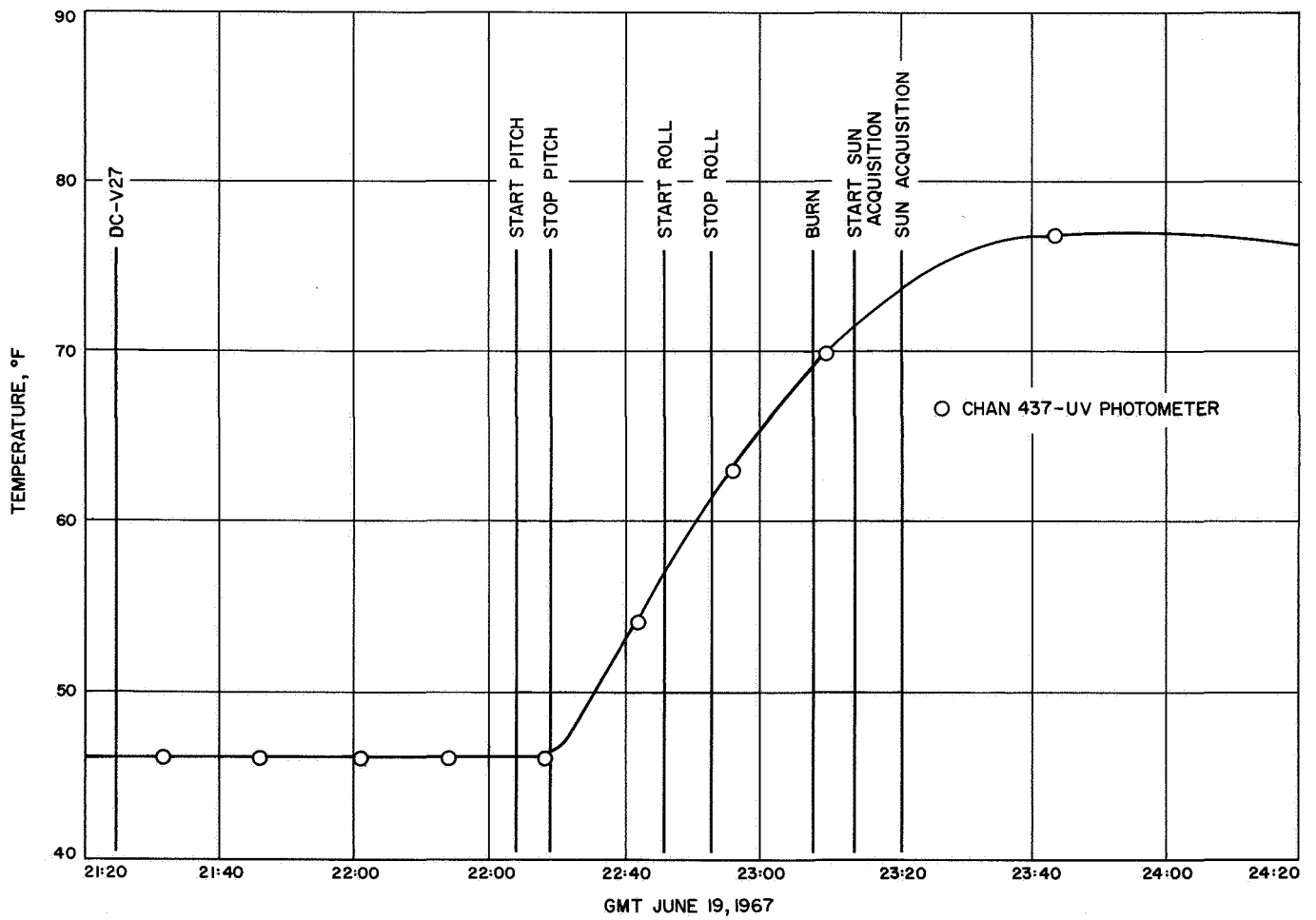


Fig. 54. Midcourse transient temperatures for UV photometer

C. Encounter

Analytical predictions of spacecraft temperature transients due to the effect of the planet were made, but engineering flight data were preempted by science at this time. Consequently, no comparison can be made. The closest point of approach to the surface of Venus was 2544 smi, and the resultant spacecraft heating was only a few degrees in the bus.

D. Cruise

The results obtained from individual telemetry channels are discussed below.

a. Bus measurements. An estimate of the error sources in the JPL 10-ft space simulator test setup indicated that test temperatures were on the order of 2°F high for earth modes and 3°F high for Venus modes. The test data for the flight spacecraft were corrected by these amounts, yielding the flight predictions of Table 5. In the worst case, the uncertainty in these predictions was $\pm 10^\circ\text{F}$, but the probable error was believed to be within $\pm 5^\circ\text{F}$. As it turned out, the average bus temperature was 1° to 2°F above prediction for most of the flight. The maximum deviation for any measurement was 4°F. Since the flight data was about midway between prediction and simulator data, it might appear that the simulator data was over-corrected. But from the data received after encounter, this is not believed to be so.

To obtain the best possible predictions for the remainder of the flight, the prelaunch predictions just described were revised after launch on the basis of near-earth data. These postlaunch predictions, which are the smooth curves shown in Figs. 15 through 35, were computed in the following way: The earth-to-Venus temperature rise observed in space simulator tests was added to the near-earth flight temperature to obtain the expected Venus temperature. The bus temperatures were assumed to be adequately described by a heat balance of the form $\epsilon T^4 = C_1 S + C_2$ where S is the solar intensity, ϵ is the effective emittance of the louvers at the corresponding temperature, and C_1 and C_2 are arbitrary constants. This equation neglects radiation and conduction within the bus, but is accurate for describing average or typical temperature behavior. The unknown constants C_1 and C_2 were obtained by substitution of appropriate data for the known earth temperature and the expected Venus temperature. By a comparison of flight data with these predictions, it is seen that typical bus temperatures ran slightly warmer than these nominal levels, until after

encounter when the actual temperatures tended to be somewhat cooler than nominal. The distortion in the curve shape is probably caused by an inaccurate representation of louver behavior. Possibly the assumed emittance-temperature function was wrong, or bearing friction retarded the opening of the blades slightly as the temperature rose. In any case, by the time telemetry was lost in late November 1967 the bus temperature was almost exactly at the levels which would have been expected before launch. This fact tends to verify the assessment of space simulator conditions. In view of the size of test errors, the agreement of flight data with preflight estimates is remarkable.

b. Solar panels. Flight predictions were based on *Mariner IV* flight data, taking into account the electrical energy withdrawn from the panels and dissipated by the spacecraft. No account was taken of the energy dissipated in the zener diodes. Near the earth, where the diodes dissipated about 230 W, the effect was to lower the panel temperatures by 8° to 10°F and raise the spar temperature by 40°F. At Venus, when panel voltage dropped to the point where the zeners were no longer firing, the panels and the spar were very near nominal temperatures. The temperature of the solar cell output transducer ($I_{sc}-V_{oc}$) was monitored to assist in interpreting the data from this cell. Its temperature, cooler than the panel average, was due to its location in an area with a relatively low solar absorptance near the panel edge.

c. Attitude control jet assemblies. The temperature predictions for these assemblies were made on the basis of type approval (TA) test results in the JPL 10-ft space simulator. Agreement with flight data was reasonably good. One interesting aspect of the postlaunch predictions bears mentioning, however. These predictions were generated by assuming that the assemblies were isothermal, with their only heat input obtained from the sun. For this case the heat balance is an equation of the form $kT^4 = S$, where k is a constant which depends on design and radiative properties. Given the initial flight temperature, k can be computed and temperatures obtained as a function of solar intensity (or solar distance). For non-isothermal sun-dependent items (i.e., when finite conduction resistance exists), the above relation is incorrect. When the solar intensity is increased, sunlit portions of such an item are warmer than predicted by this equation, while shaded portions are cooler. For the gas jet assemblies the transducers were in the latter category. The results are apparent when the flight data are compared with the postlaunch predictions.

d. *Lower thermal shield.* In the absence of any change in radiative properties, this temperature would be very nearly proportional to the fourth root of the solar intensity. A small correction is necessary to account for the fact that the transducer temperature is really somewhere between the temperature of the first and second layers of the shield rather than exactly at the temperature of the first (Teflon) layer. This effect causes a maximum decrease of 4° or 5°F in the measured earth-to-Venus temperature rise as compared with that computed for an idealized adiabatic flat plate; it was neglected in the postlaunch prediction. Table 5 and Figure 40 show that the temperature rise in flight exceeded simulator results and postlaunch predictions, respectively. This departure was caused by a darkening of the Teflon outer layer of the shield. Figure 41 shows the increase in absorptance during the flight, omitting the relatively small correction discussed above.

The 10°F difference in temperature between flight and the simulator test for near-earth solar intensity was probably caused by a disproportionately large infrared component in the solar simulator.

e. *Plasma probe.* Near earth the flight temperature and corresponding simulator temperature were the same for this instrument. By encounter time, the probe temperature had risen 18°F above prediction. This increment was no doubt the result of (1) increased infrared radiant heating on the white sides of the probe caused by the degradation of the lower shield, and (2) increased reflected solar heating resulting from a darkening of the white paint on the sides of the probe.

f. *Primary sun sensor.* When temperature stabilization was reached after launch, the primary sun sensor temperature was very close to prediction — about 2°F warm. As the flight progressed, the temperature increased more rapidly than expected. At encounter the deviation from prediction had reached 23°F, and the sensor temperature continued to rise abnormally after encounter.

Data were obtained during TCM testing to evaluate the effect of increasing the heat input to the primary sun sensor assemblies. From these data, it was deduced that an incremental heat input of 3.2 W at Venus would produce the 23°F discrepancy observed. About 0.7 W of this total was due to the darkening of the lower thermal shield, which increased the infrared input to the sides of the assembly and pedestal. The darkening of the white paint on the sides of the pedestal no doubt also contributed to an increased reflective solar input. The

remaining input, something less than 2.5 W, was probably the result of one or more of the effects listed:

- (1) Increase in diffuse component of shield and shade reflectance.
- (2) Shift in shade position.
- (3) Decrease in conduction coupling to bus.

The necessary change in each of these parameters to produce a 2.5 W input was calculated. Any one of these changes would produce a 2.5 W input:

- (1) Diffuse reflectance (r_d) increased from 0.3 to 0.63.
- (2) Readjustments of the shade position doubled the reflected input.
- (3) The shade position relative to the pedestal moved 1 in. closer to the bus.
- (4) The conduction coupling to the bus decreased to zero.

Other possibilities, considered less likely, are flaking paint, transducer detachment, or space simulator test inaccuracies. By a process of elimination, it seems most probable that optical changes in the Teflon or some shifting of the shade position, or both, increased the heat input to the sides of the pedestal and sensor assembly.

g. *Low gain antenna mast.* Low temperature spacecraft components are very sensitive to extraneous heat inputs in space simulator tests because small changes in heat input cause large temperature changes. The same change in heat flux which produces a 10°F ΔT at 70°F will produce a 32°F ΔT at -100°F. For this reason (and others), it is to be expected that the heavily corrected space simulator data which yield temperature predictions for these items will have sizable uncertainties, say $\pm 30^\circ\text{F}$. The agreement between prediction and flight data for the low gain mast is therefore fairly good.

The mast (waveguide) temperature proved to be sensitive to RF losses. The temperature increased by 11°F when the TWT amplifier replaced the cavity amplifier, and the temperature dropped by 19°F when the switch to the high gain antenna occurred. About 4°F of the first temperature change was caused by the temperature change in bay 6. The remaining ΔT was the result of power loss changes in the waveguide.

h. *Upper thermal shield.* This measurement was intended primarily to yield comparative data between

flight and space simulator conditions, and to provide some idea of shield performance. The heat balance in flight can be written as

$$\epsilon\sigma T_S^4 = K_1(\sigma T_B^4 - \sigma T_S^4) + K_2S$$

radiation from shield	input from bus	external input
--------------------------	-------------------	-------------------

where K_1 and K_2 are constants. It is assumed that all external heating is directly proportional to the solar intensity S , and that heat transfer through the upper shield occurs by radiation only. When the flight temperature data near the earth and Venus is substituted into the equation, the values for K_1 and K_2 can be obtained. On this basis, the heat loss from the bus was computed to be nearly constant at 0.78 W/ft², and the effective emittance of the shield was 0.02. These values must be regarded as upper limits, since part of the heat loss at the transducer was contributed by heat conduction down the leads. A more significant outcome of these calculations is the ability to deduce space simulator heat inputs to the upper shield. The external heat input (radiation from shield minus input from bus) was calculated to be 1.3 W/ft² at Venus intensity. These levels are about twice what would be expected from previous evaluations of stray radiation. The increase was no doubt caused by the presence of the spacecraft and associated test hardware in the simulator.

i. UV photometer. The temperature-time history of this instrument was as expected throughout flight, except for a 2° to 3°F temperature increase after the bit rate change (33½ bits/s to 8½ bits/s). This temperature increase was the result of a power change of about 0.5 W. The change was normal, but its effect had been overlooked in preflight testing.

j. High gain antenna. The temperature prediction for the antenna, based on analysis, proved to be about 25°F low. Considering the low temperatures involved, such a discrepancy is not surprising. The temperature varied in flight in sun-dependent fashion, since the heat input was primarily supplied by radiation from the solar panels. The position change (APAC) at encounter reduced the radiative coupling between the high gain and upper shield, and increased the coupling between the high gain and solar panels. These changes lowered the upper shield temperature 12°F and raised the high gain temperature 21°F. These seemingly dramatic changes were actually

caused by very low level changes in energy inputs. For small changes in heat input, ΔT is proportional to $\Delta q/T^3$. Thus the low temperatures magnified the effect of the radiant input change, as was also true for the temperature prediction discrepancy.

VIII. Conclusions and Recommendations

The thermal design philosophy and implementation were adequate, as was borne out by the successful flight results. For this spacecraft, the relative emphasis of test and analysis produced a conservative and reliable design. The project organization was workable. Further clarification of the purpose and relationship of various temperature limits (FA, TA, design, failure) would be helpful.

It can be concluded that the conversion from *Mariner* Mars 1964 to *Mariner* Venus 67 was less difficult than producing the entire design and development from scratch. The *Mariner* thermal design for the bus depends on solar isolation; once this isolation was provided, the louver and side shielding arrangement was usable intact. The new techniques used to isolate the bus from solar heating proved effective. *Mariner V* had to be — and was — less affected by solar heating than any previous spacecraft of the series. The lower thermal shield, the deployable sun shade, and the solar panel cutouts all contributed to this sun-independence.

All temperature control hardware performed as designed. Behavior in space was essentially identical to behavior in ground testing. Subsystem hardware inherited from *Mariner* Mars 1964 was generally unaffected by age. The louver hysteresis effects noted in flight were substantially less than those permitted by design specifications; the effect is mainly of interest in defining the ultimate limits of temperature predictability.

The superinsulation shield design for this spacecraft was thermally and operationally adequate. Heat leaks were small and repeatable. The remarkable insulating qualities reported for calorimeter test specimens are neither achievable nor necessary on *Mariner* type shields. The average shield properties are controlled by heat leaks through penetrations, seams, attachments and other thermal imperfections. The absolute value of the heat leak is less important than the uncertainty (or variation) in that value. The *Mariner* Venus 67 design rightly concerned itself with this problem and with rendering the shields operationally compatible with the spacecraft to

which they were attached. The simplified installation and removal of the upper shield was particularly worthwhile.

The coatings used for optical property control functioned normally. Preflight durability, a prerequisite for selecting the coatings, was acceptable. The only ground difficulties of note were deterioration of the vacuum-deposited aluminum on the magnetometer sphere and corrosion of magnesium surfaces through the DOW-7 coating. Flight ultraviolet degradation of the Teflon on the sunlit shield and of the white paint on the plasma probe, sun sensor pedestals, and the TCRs indicates that the *stable white* surface is still nonexistent. It is therefore advisable to avoid the use of white coatings for critical sunlit surfaces whenever possible.

The success of the thermal design depends greatly on the space simulator in which it is tested. For this program the timely upgrading of the solar simulator and an improved understanding of the test environment produced accurate flight temperature predictions. The importance of thorough simulator checkout and solar intensity monitor calibration can hardly be overstressed. The measurement of solar intensity continues to be a problem, but the state-of-the-art has improved since the *Mariner* Mars 1964 mission. Space simulation for the *Mariner* Venus 67 spacecraft was good, but small appen-

dages, such as the magnetometer, require careful data analysis and test-error correction.

The most valuable features of the space simulator tests of the temperature control model were the initial subsystem checkout, failure mode data, and parametric investigation. Detailed design refinements are not justified, since the TCM is not likely to be exactly like the final spacecraft design, anyway. The 10% error in the estimate of dissipated power for the TCM was costly in time, money, and applicability of TCM data. Future programs should take every precaution to prevent such an error, but parametric data and design margin must be provided in case a thermal design change is later required. A small test facility for space simulation testing of individual assemblies would be valuable. Isolated appendages such as the magnetometer cannot be adequately tested during TCM and system level space simulator tests. A one-fifth scale version of the 10-ft space simulator would solve this dilemma.

The upgrading of the computer thermal model, from test results, is essential for the accuracy of the model, and the process is helpful in obtaining a better understanding of the spacecraft's thermal characteristics. The *Mariner* Venus 67 experience indicated that previously obtained louver efficiency data was in error.

Appendix A

Project Organization

The thermal design, analysis, and test of the *Mariner* Venus 67 spacecraft were performed by the temperature control group of the Engineering Mechanics *Mariner* Development Section. This group consisted of five engineers throughout most of the life of the project: one cognizant hardware engineer, one mechanical test support engineer, and three thermal specialists who shared the design, analysis, and test tasks. Since the *Mariner* Development Section was completely project-oriented, the same engineers were active with the evolution of the spacecraft from preliminary design to flight data analysis.

The *Mariner* 67 Project organization is shown in Fig. A-1. The detailed requirements for temperature control were established through interfaces with cognizant subsystem personnel; the necessary design provisions were made in the spacecraft configuration, structure, packaging, and thermal control hardware. The latter was included in the temperature control subsystem; the remaining design features were under the cognizance of other groups within the engineering mechanics division.

The temperature control group had important contact with all three members of the spacecraft system manager's staff during the development of the project. Systems aspects of the spacecraft design were directed by the system engineer and approval for design changes were obtained through him by the cognizant temperature control engineer. The environmental requirements engineer specified certain test levels for simulator tests, flight approval tests, and type approval tests; cooperation in the definition and monitoring (in the case of flight simulator tests) of these levels between this engineer and temperature control personnel also proved vital.

The Space Flight Operations (SFO) organization, not shown in Fig. A-1, was concerned with spacecraft performance analysis and control (SPAC) in flight. Temperature control personnel were active in these efforts during flight operations.

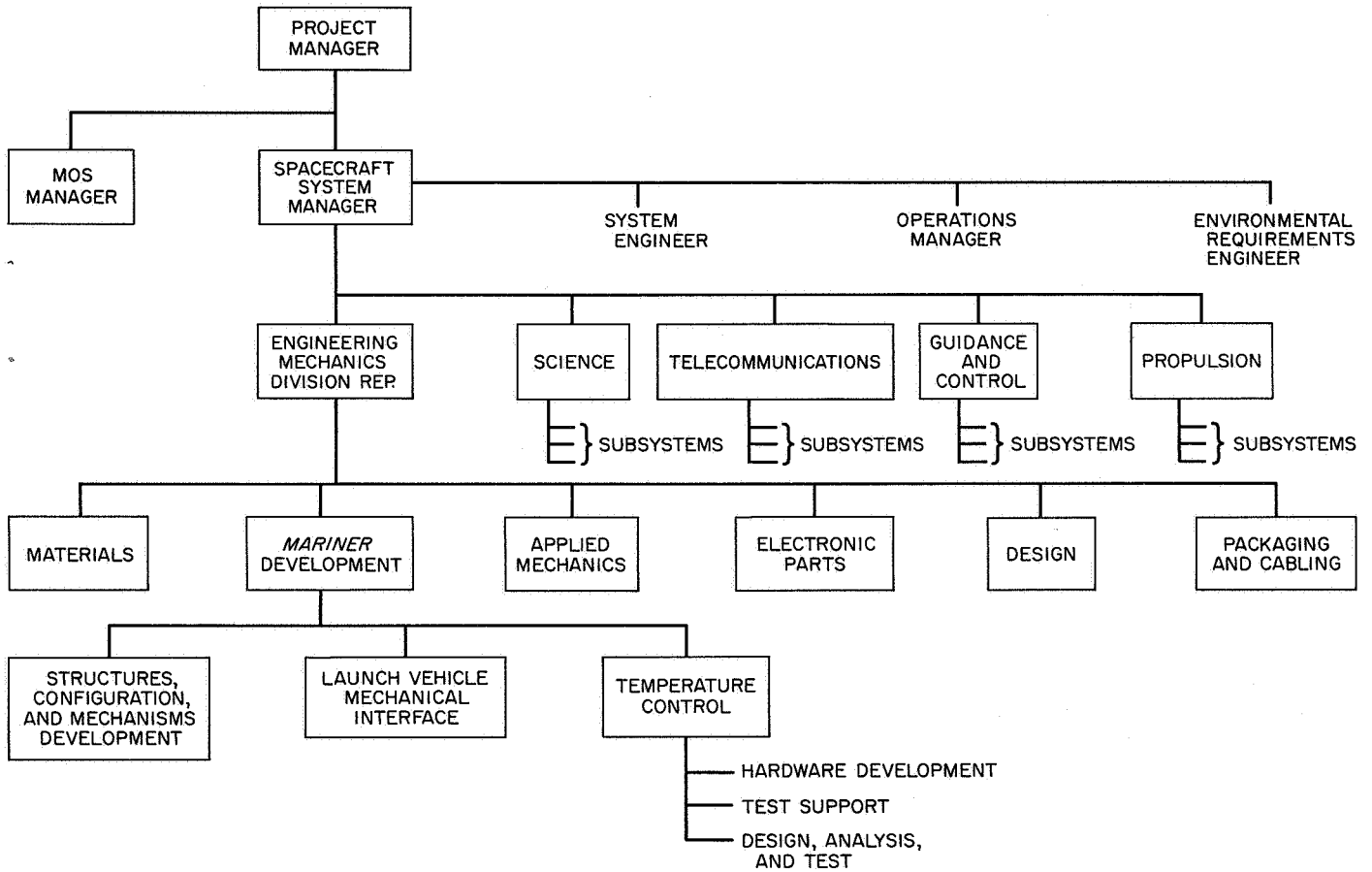
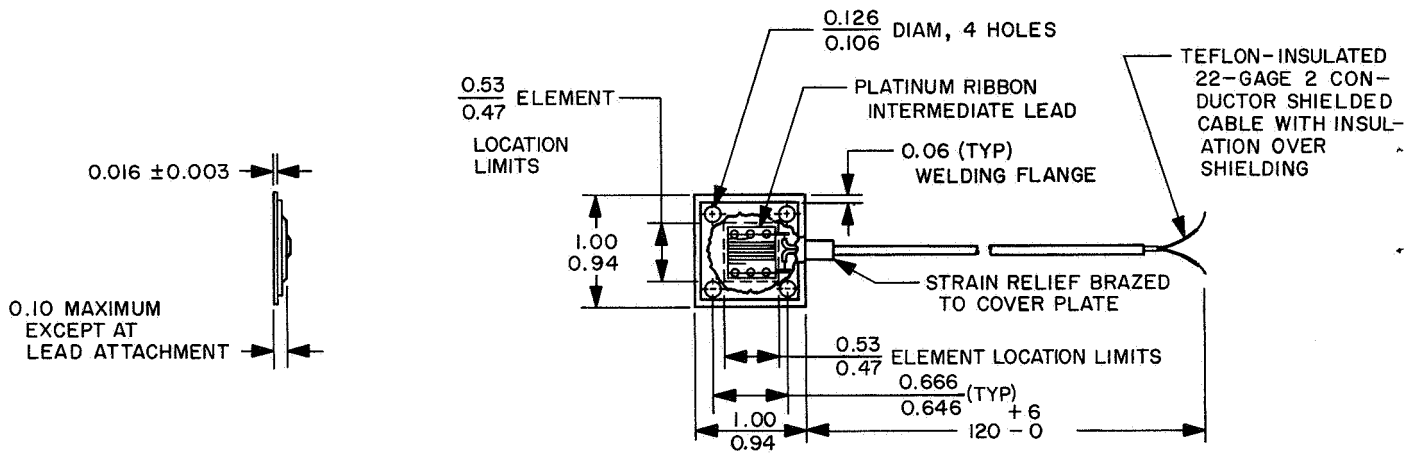


Fig. A-1. Project organization

Appendix B

Flight Transducer Locations



ALL MEASUREMENTS SHOWN IN INCHES

NOTES

(1) MATERIAL

COVER-PLATE MATERIAL, TYPE 302 SS

BASE-PLATE MATERIAL, EPOXY FIBERGLAS

ENTIRE CAVITY PRECOATED WITH HARD HIGH-TEMPERATURE INSULATION AND POTTED WITH EPOXY AFTER WINDING IS ASSEMBLED

(2) OPERATING RANGE

-300° TO +300°F

Fig. B-1. Temperature transducer

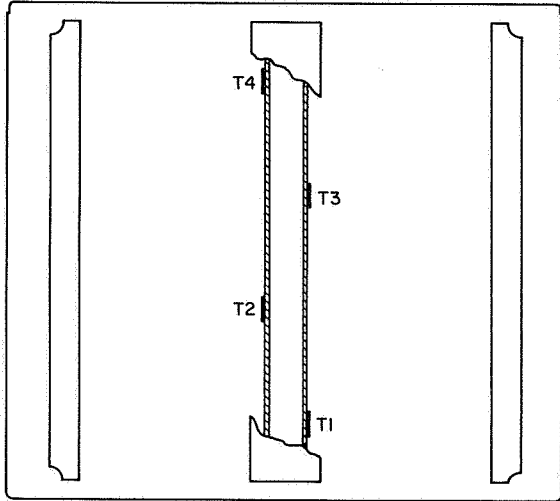
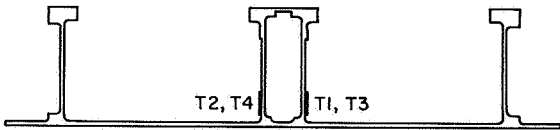
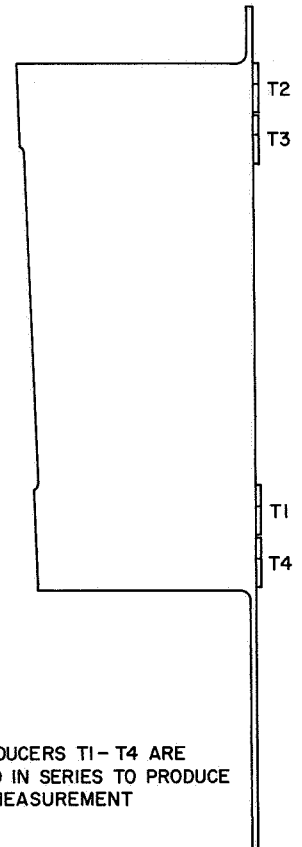
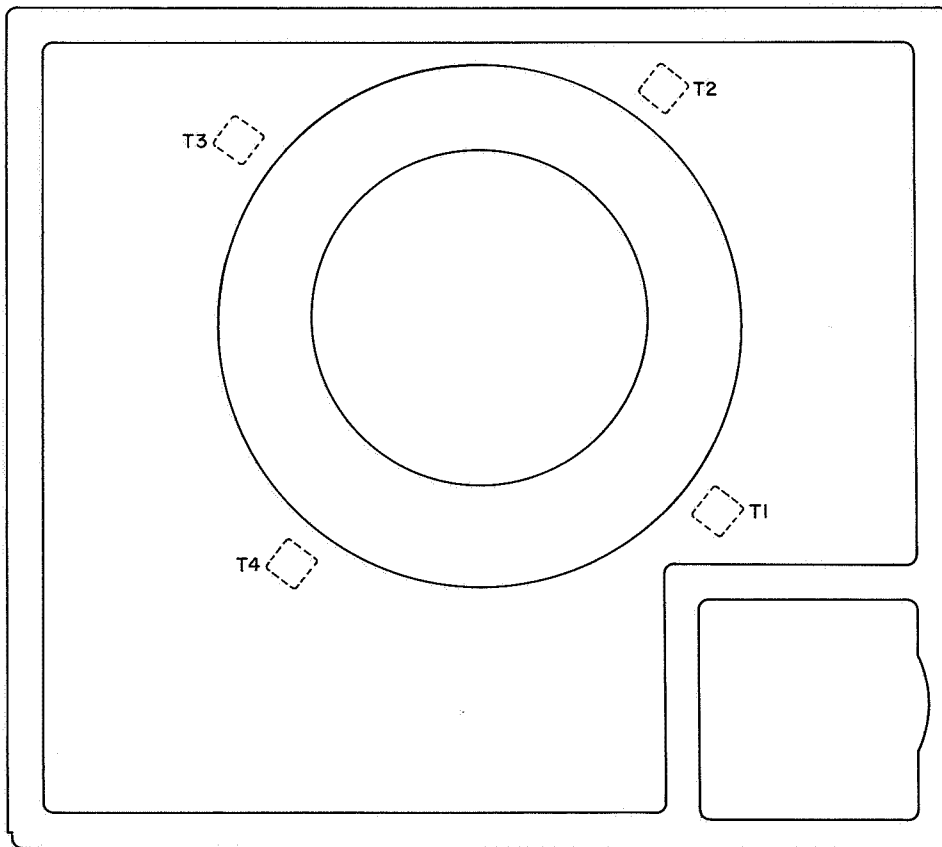


Fig. B-2. Typical electronics assembly installation

BAY	CHAN
1	401
3	402
4	423
5	404
6	405
7	426



NOTE
 TRANSDUCERS T1-T4 ARE CONNECTED IN SERIES
 TO PRODUCE AVERAGE TEMPERATURE MEASUREMENT



NOTE
 421 TRANSDUCERS T1-T4 ARE
 CONNECTED IN SERIES TO PRODUCE
 AVERAGE MEASUREMENT

Fig. B-3. Bay 2 shear plate

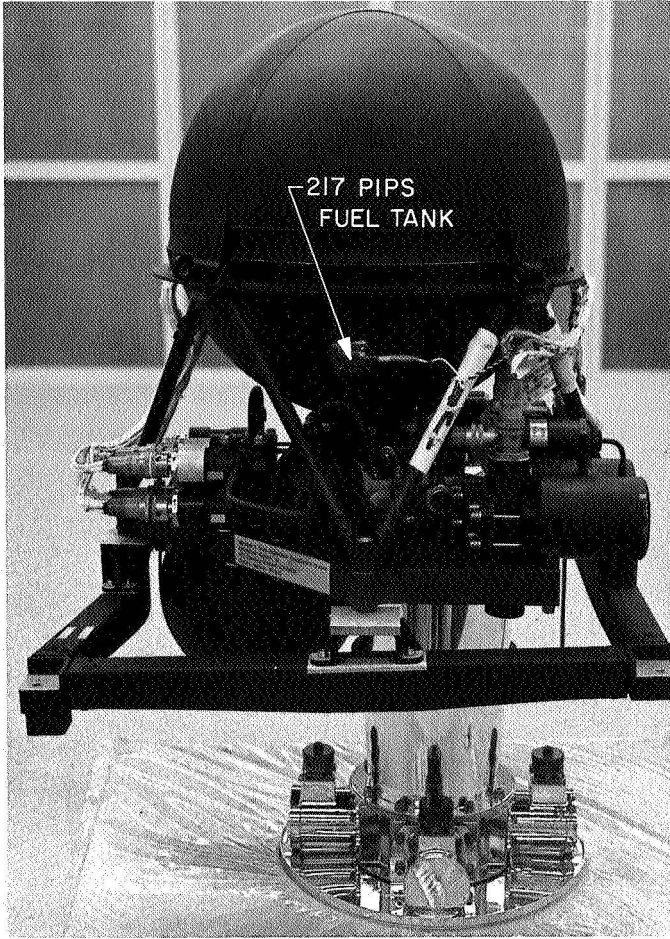


Fig. B-4. Propellant tank

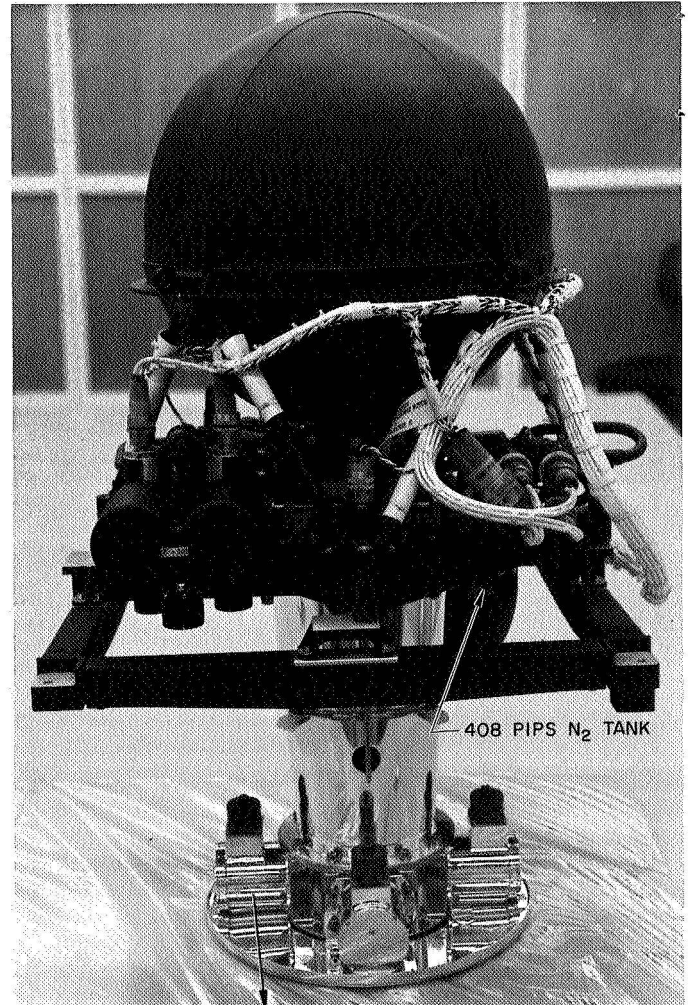


Fig. B-5. Propulsion nitrogen tank

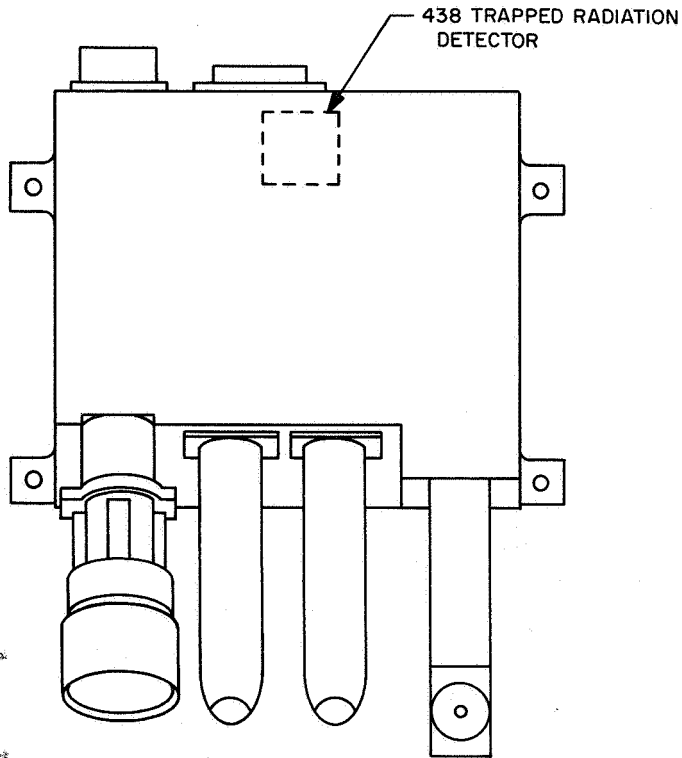


Fig. B-6. Trapped radiation detector

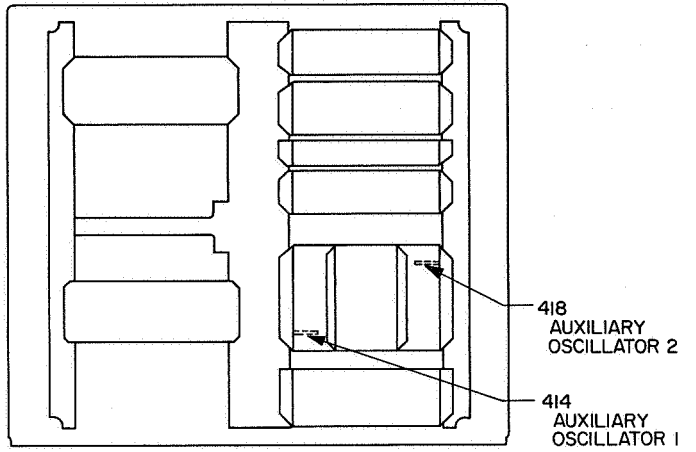


Fig. B-8. Electronics assembly VI

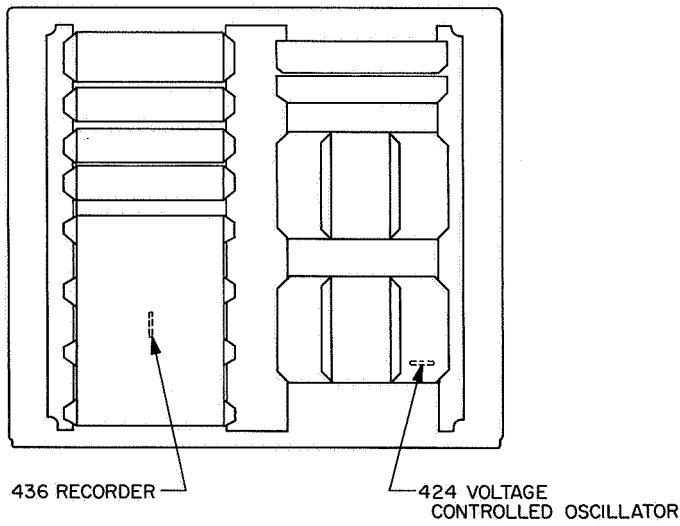


Fig. B-7. Electronics assembly V

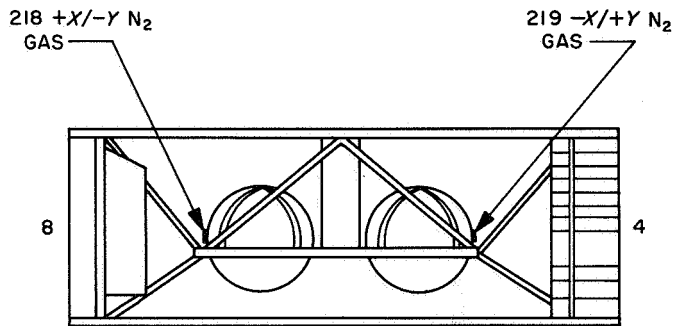


Fig. B-9. Attitude control nitrogen tanks

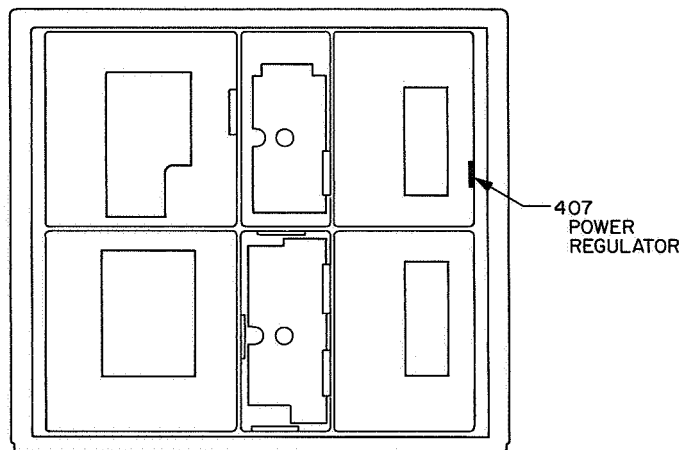


Fig. B-10. Electronics assembly VIII

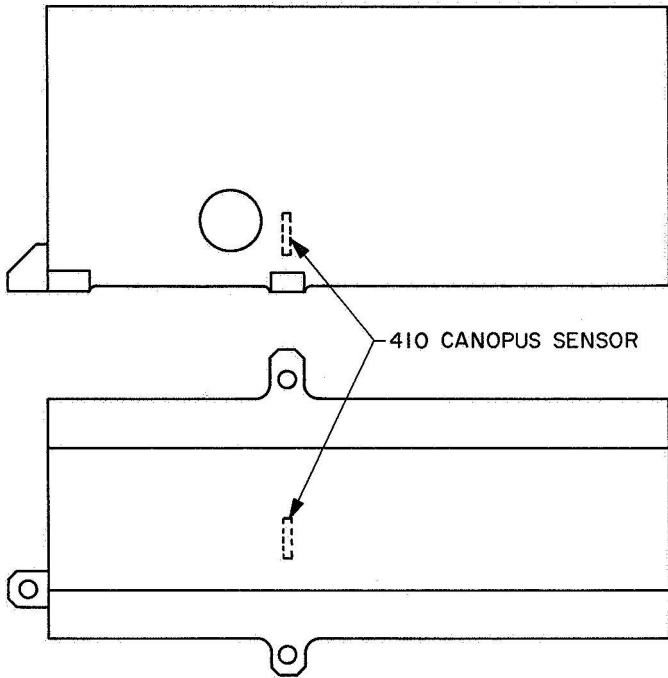


Fig. B-11. Canopus sensor

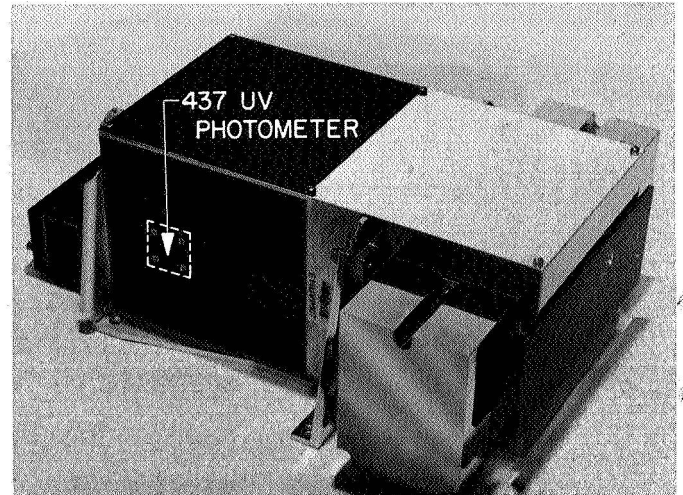


Fig. B-13. UV photometer

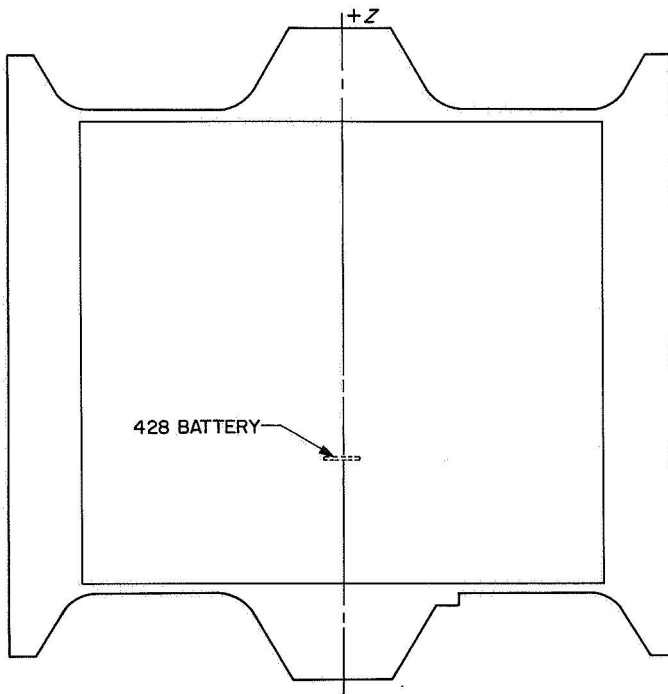


Fig. B-12. Battery

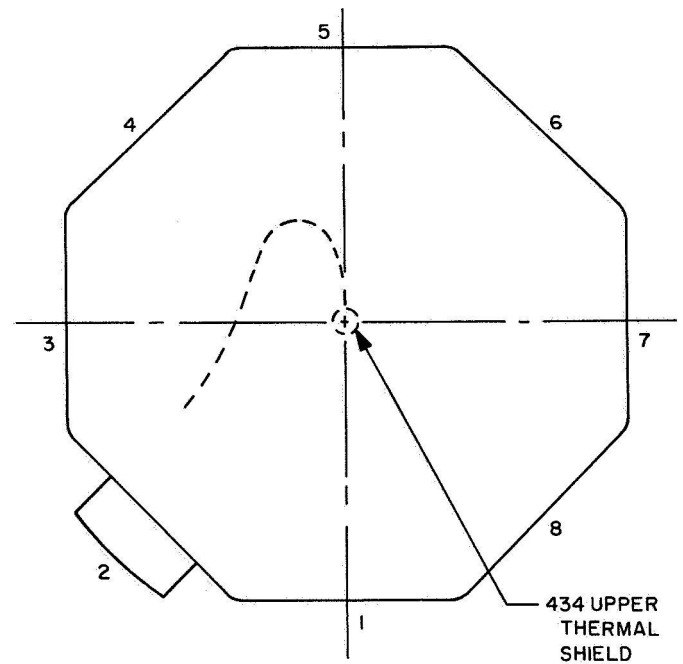


Fig. B-14. Upper thermal shield

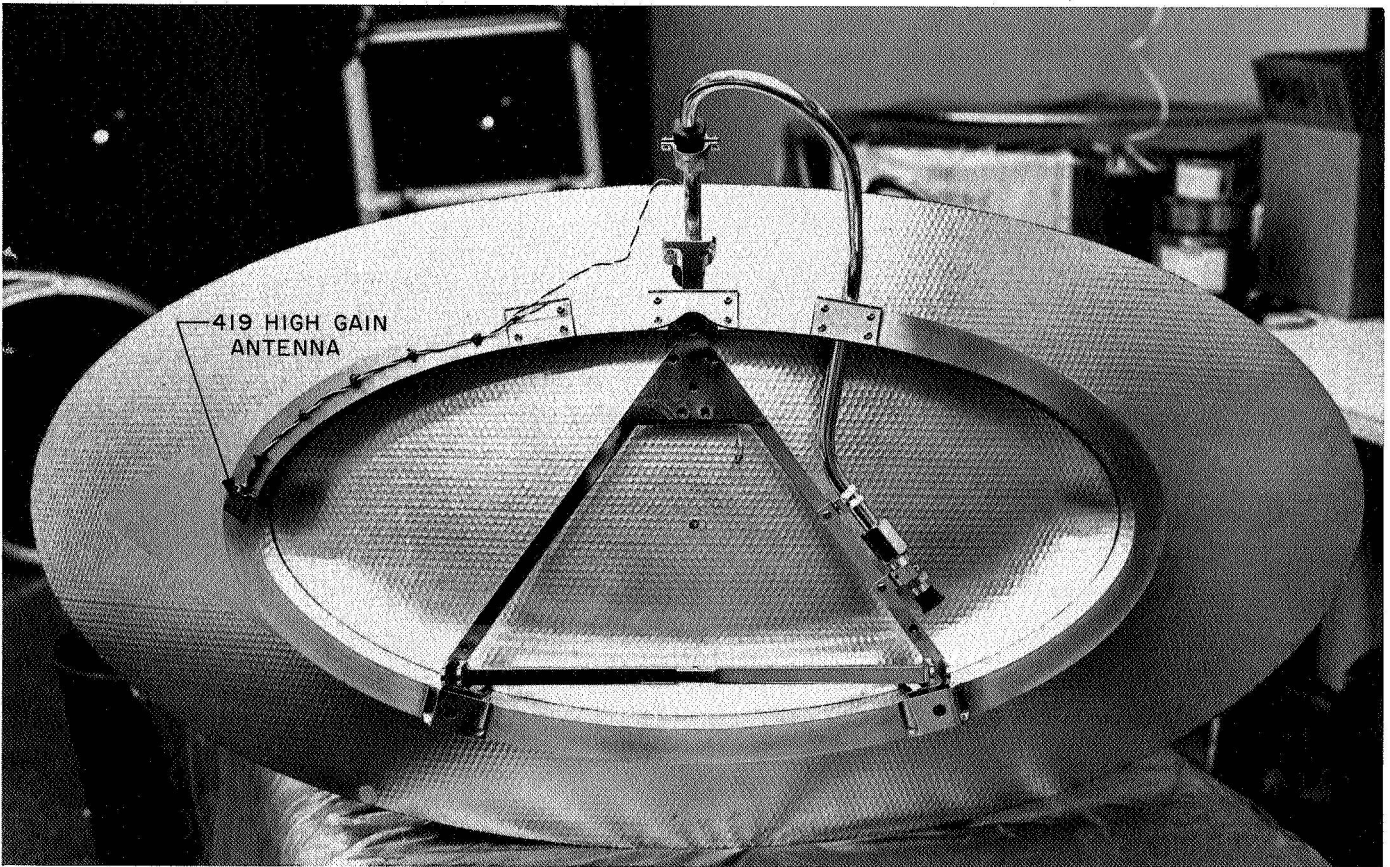


Fig. B-15. High gain antenna

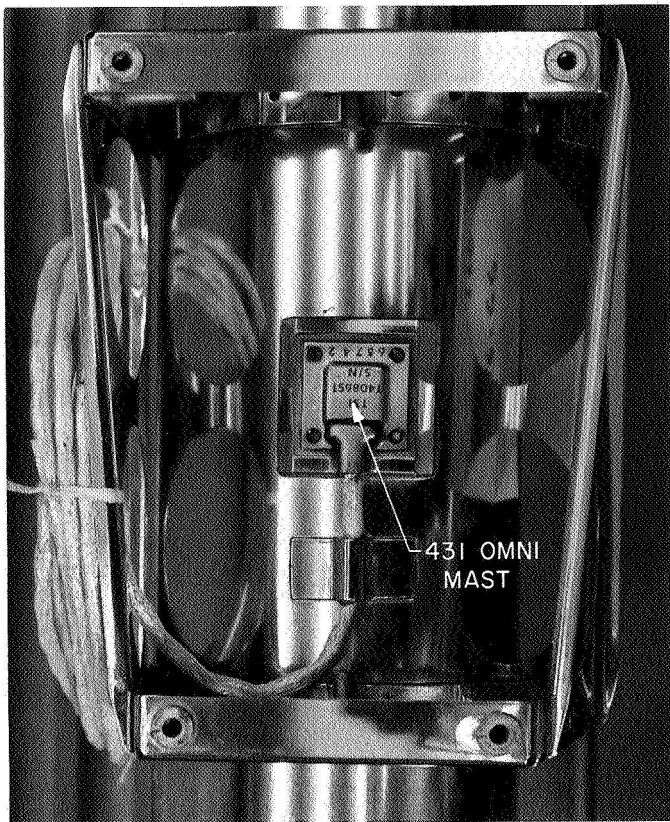


Fig. B-16. Omni mast

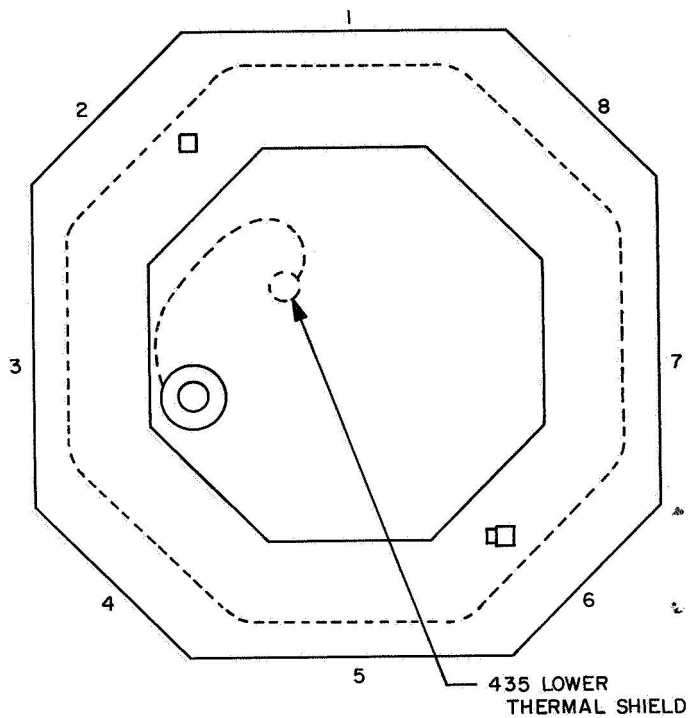


Fig. B-18. Lower thermal shield

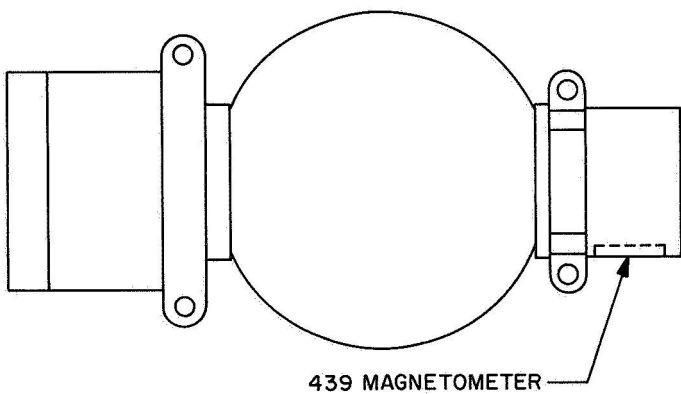


Fig. B-17. Magnetometer

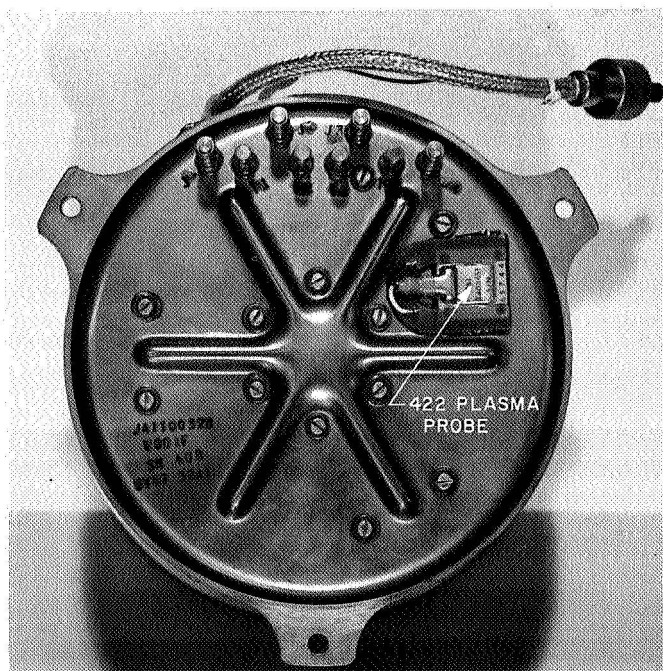


Fig. B-19. Plasma probe

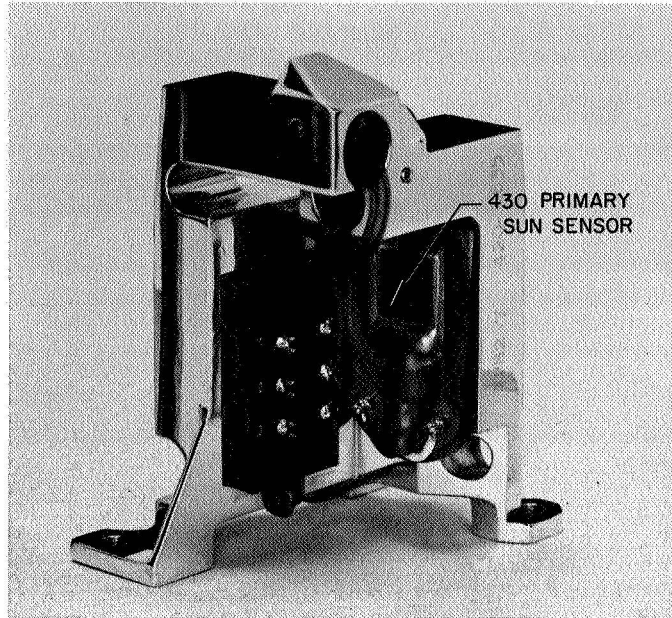


Fig. B-20. Primary sun sensor

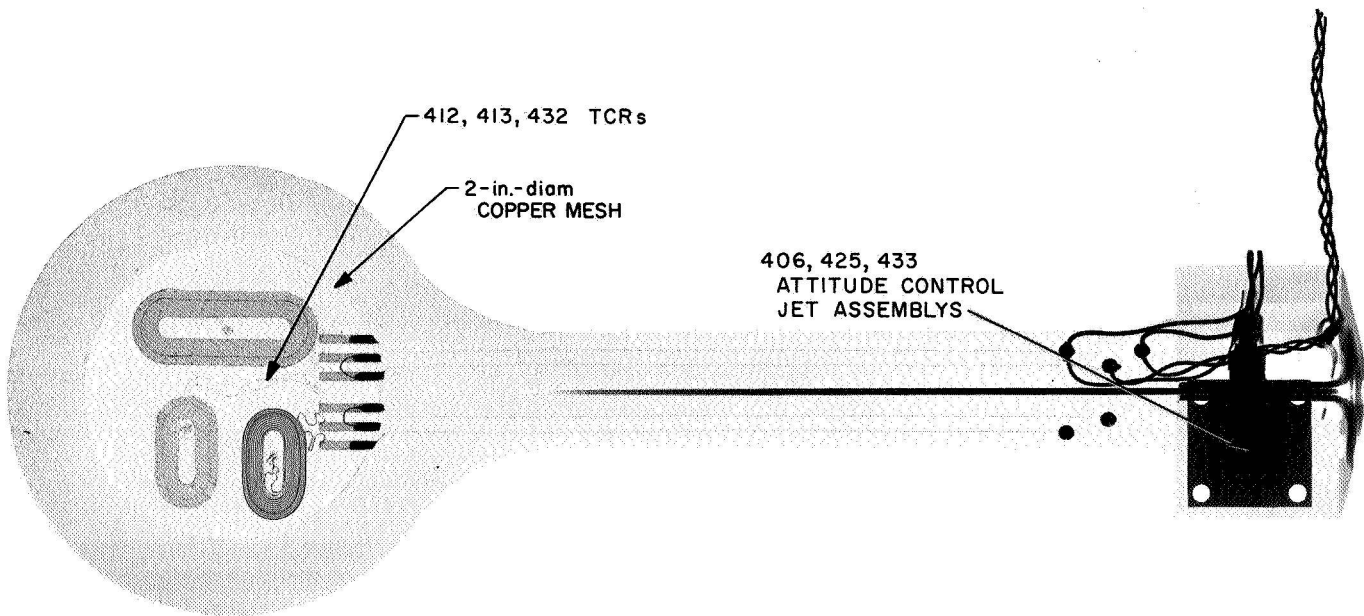


Fig. B-21. Temperature control references

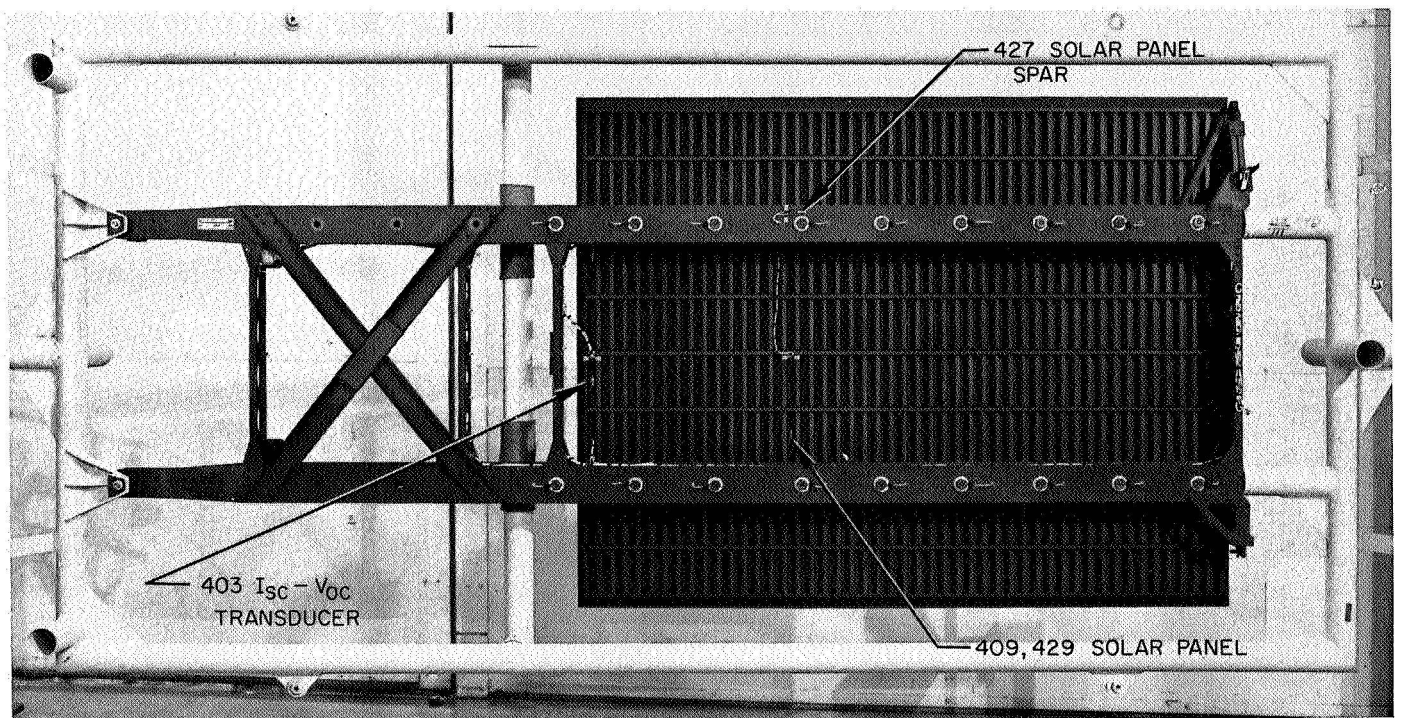


Fig. B-22. Solar panel

References

1. *Mariner Venus 67 Final Project Report: Volume I. Launch Through Midcourse Maneuver*, Technical Report 32-1203. Jet Propulsion Laboratory, Pasadena, Calif., June 15, 1968.
2. *Mariner Venus 67 Final Project Report: Volume II. Midcourse Maneuver Through Post-Encounter*, Technical Report 32-1203. Jet Propulsion Laboratory, Pasadena, Calif. (to be published).
3. *The Mariner Venus 1962 Final Project Report*, NASA SP-59, National Aeronautics and Space Administration, Washington, D.C., 1965.
4. *Mariner Mars 1964 Project Report: Mission and Spacecraft Development: Volume I. From Project Inception Through Midcourse Maneuver*, Technical Report 32-740. Jet Propulsion Laboratory, Pasadena, Calif., Mar. 1, 1965.
5. *Mariner Mars 1964 Project Report: Mission and Spacecraft Development: Volume II. Appendixes*, Technical Report 32-740. Jet Propulsion Laboratory, Pasadena, Calif., Mar. 1, 1965.
6. Lewis, D. W., Miller, D. C., and Dumas, L. N., *Mariner Mars 1964 Temperature Control Subsystem*, Technical Report 32-957. Jet Propulsion Laboratory, Pasadena, Calif., Sept. 15, 1967.
7. *Mariner Mars 1964 Project Report: Spacecraft Performance and Analysis*, Technical Report 32-882. Jet Propulsion Laboratory, Pasadena, Calif., Feb. 15, 1967.
8. Carroll, W., Coyle, G. G., and von Delden, H., *Mariner Mars 1964 Temperature Control Hardware Design and Development*, Technical Report 32-955. Jet Propulsion Laboratory, Pasadena, Calif., June 1, 1967.
9. Carroll, W. F., "Mariner V Temperature Control Reference Design, Test, and Performance," Paper presented at the AIAA 3rd Thermophysics Specialists Conference, Los Angeles, Calif., June 24-26, 1968.
10. Ragsdale, G. C., and Mesnard, D. C., *Mariner Venus 67 Spacecraft Environmental Test Results*, Technical Report 32-1249. Jet Propulsion Laboratory, Pasadena, Calif., June 15, 1968.
11. Lund, D. E., *The 10-ft Space Simulator at the Jet Propulsion Laboratory*, Technical Report 32-1231. Jet Propulsion Laboratory, Pasadena, Calif., Dec. 15, 1967.